



**FACULTY
OF MATHEMATICS
AND PHYSICS**
Charles University

BACHELOR THESIS

Václav Štěpánek

**Atmospheric Neutrino Oscillations in
the Hyper-Kamiokande Experiment**

Institute of Particle and Nuclear Physics

Supervisor of the bachelor thesis: RNDr. Ing. Bedřich Roskovec,
Ph.D.

Study programme: Physics

Study branch: Physics

Prague 2023

I declare that I carried out this bachelor thesis independently, and only with the cited sources, literature and other professional sources. It has not been used to obtain another or the same degree.

I understand that my work relates to the rights and obligations under the Act No. 121/2000 Sb., the Copyright Act, as amended, in particular the fact that the Charles University has the right to conclude a license agreement on the use of this work as a school work pursuant to Section 60 subsection 1 of the Copyright Act.

In date

Author's signature

Title: Atmospheric Neutrino Oscillations in the Hyper-Kamiokande Experiment

Author: Václav Štěpánek

Department: Institute of Particle and Nuclear Physics

Supervisor: RNDr. Ing. Bedřich Roskovec, Ph.D. - Institute of Particle and Nuclear Physics

Abstract: This thesis focuses on the neutrino physics. The main theme of the thesis was the next generation water Cherenkov experiment Hyper-Kamiokande, which will play key role in the δ_{CP} measurement through the accelerator neutrinos. However, the atmospheric neutrinos can significantly boost its sensitivity. In this thesis, we have develop a simplified model for atmospheric neutrino flux prediction and estimated the number of events the Hyper-Kamiokande experiment will detect. We have compared this result with the measurement of ts predecessor Super-Kamiokande.

Keywords: Hyper-Kamiokande, atmospheric neutrinos, neutrino oscilation

Contents

1	Introduction	2
2	Neutrino Oscillation	5
2.1	General Formalism of Neutrino Mixing	5
2.2	General Formalism of Neutrino Oscillation	5
2.3	Two-neutrino Oscillation in Vacuum	8
2.4	Three-neutrino Oscillation in Vacuum	8
2.5	Matter Effect	10
3	Neutrino Sources and Measurement	12
3.1	The θ_{12} and Δm_{21}^2 Measurement	12
3.2	The θ_{23} and Δm_{32}^2 Measurement	14
3.3	The θ_{13} and Δm_{31}^2 Measurement	17
3.4	The δ_{CP} Measurement	19
4	Prediction of Neutrino Flux at Hyper-Kamiokande	23
4.1	Production of Neutrinos in the Atmosphere	24
4.2	Probability, Oscillation Parameters and Matter Effect	26
4.3	The Earth Model and the Oscillated Fluxes	28
4.4	The Hyper-Kamiokande Experiment	31
4.5	Fluxes, Predicted Number of Events and Discussion	32
5	Conclusions	38
	Bibliography	39
	List of Figures	41
	List of Tables	43

Chapter 1

Introduction

Neutrino is a particle predicted in 1930 by W. Pauli based on observed β -decay spectrum. When emission spectrum of electron was measured, just monoenergetic peak was expected. Surprisingly, continuous spectrum was observed, what indicated another particle in the decay. This particle was originally called neutron and later neutrino, because of zero charge and zero mass (or at least very small compared to electron). Due to its low reactivity, it took more than 25 years to actually prove its existence.

In the Standard Model (SM) of particle physics, neutrinos are actually massless neutral elementary particles with spin one half and interacting only via weak interaction, so called neutral leptons. Leptons are particles, which do not feel strong interaction, such as quarks. Thanks to this fact, neutrino has significantly smaller cross section compared to any other elementary particle, what makes it very difficult to detect. From experimental results, it is known, that neutrinos have three different flavours corresponding to three charged leptons. They are denoted as ν_e for electron neutrino, ν_μ for muon neutrino and ν_τ for tau neutrino. Every neutrino or antineutrino in reaction acts together with the charged lepton or the antilepton of the same flavour, so lepton number is conserved.

Neutrinos were experimentally discovered in 1956 by C. Cowan and F. Reines [1]. They in fact measured antineutrinos created in nuclear reactor from β -decay of daughter nucleus containing extra neutrons produced by nuclear fission of heavy elements. Actually, the neutrino is the only particle for which an antiparticle has been confirmed earlier than a particle. Reines earned the Nobel Prize for physics in 1995 for its discovery.

Although the neutrino was discovered, at that time, many interesting phenomena and problems were revealed. One of the problems was so called the Solar Neutrino Problem. Physicists realised that the Sun should be large source of just electron neutrinos due to thermonuclear reactions happening in the Sun's core. Prediction of neutrino fluxes from the Standard Solar Model, the Sun's luminosity and distance between Earth and Sun, was very inconsistent with the measurement made by R. Davis at the Homestake experiment in 1960s. Measured flux was close to a one third of predicted flux [2]. This problem took over thirty years until the Solar Neutrino Problem was solved by discovering MSW (Mikheyev–Smirnov–Wolfenstein) matter effect, which predicted a flavour change of neutrinos [3].

Another interesting phenomenon is the neutrino oscillation. As it has been

said, lepton number in the SM interactions is conserved. But the Sudbury Neutrino Observatory (SNO) in Canada proved neutrino flavour transition of the solar neutrinos. SNO was a spherical heavy water Cherenkov detector and it was able to measure every type of neutrino, because of neutral current scattering with electron by Z boson exchange or similarly with neutron. When neutron kicked out from deuteron by neutrino is captured on hydrogenium atom, roughly 2.2 MeV gamma photon is emitted and it could be detected. By combination of results from neutral and even charged current, it was determined that flux from the Sun was predicted correctly, but neutrinos changed flavour [4].

One of the possible explanations was so called neutrino mixing, which means, that flavour (or active) neutrino could be composed of superposition of three neutrinos mass states. This mass states can be changed depending on the matter, where they are in. This phenomenon has few important consequences. One of the consequences is neutrino oscillation. Oscillation means, that neutrino can not only change its flavour (after some distance propagated), but eventually can change it back to the initial flavour. Experimental proof of oscillation was provided at the Super-Kamiokande experiment (or shortly Super-K) by measurement of atmospheric neutrinos in 1998 [5]. Arthur B. McDonald and Takaaki Kajita were awarded by the Nobel prize for this observation in 2015. This proof motivated number of new experiments, which had to solve several unanswered questions.

Some of these questions are resolved, but there are still remaining open questions in neutrino physics are for example neutrino hierarchy, absolute masses of mass states, θ_{23} mixing angle octant (if $\theta_{23} > \frac{\pi}{4}$ or $\theta_{23} < \frac{\pi}{4}$), Dirac δ_{CP} phase corresponding to CP violation and if neutrinos are Majorana or Dirac particles. If neutrino is Majorana particle, it mean that neutrino particle is its own antiparticle. As you will see in following text, oscillation depends only on differences of squared masses of neutrino mass states, mixing angles and potentially on so called Dirac CP phase. Roughly speaking, we can measure only the absolute value of the difference of mass states masses squared in case of difference between third and second mass and because of uncertainty of this parameter, we cannot decide, if the second mass state is heavier or lighter than the others, so we are not sure about so called hierarchy of absolute masses and absolute masses itself (there is just upper limit from the KATRIN experiment, but still not enough for absolute masses of mass states knowledge [6]). Similarly, from oscillation we are able to measure only sine squared of one double mixing angle now, so it is not clear in which octant does mixing angle belongs to. This could be measured in probability of $\nu_\mu \rightarrow \nu_\mu$ survival, but it has not been measured yet. Other parameters, such as Dirac phase, and Majorana phases are still unconstrained.

Atmospheric neutrinos are produced in the higher Earth troposphere. Particles from cosmic rays (mostly high energetic protons or heavier nuclei) from outer space interact with atmospheric atoms and create a particle shower, mostly made up from mesons such as pions, kaons among others. These mesons decay (mostly before they hit the ground) and in these processes neutrinos and antineutrinos are produced. For example π^- decay to $\bar{\nu}_\mu$ and μ , which decay to electron, ν_μ and $\bar{\nu}_e$. These different flavours are produced in specific and predictable ratio, naively estimated as two to one of number of ν_μ to number of ν_e . That means we can measure fluxes of flavour neutrino after propagation via atmosphere and the

Earth and compare measured and predicted ratio.

These fluxes are measured by Super-K. Super-K [7] is a water Cherenkov detector, cylindrical pure water tank 41 m in height and 39 m in diameter with inward facing photomultiplier tubes (PMTs) 1000 m underground to shield atmospheric μ . Cherenkov detector measure charged particles which flew through the transparent filling and which reached so called phase velocity. Phase velocity is another name for speed of light in the environment (in water in the Super-K case) and reaching this minimal velocity is crucial supposition of Cherenkov-light emitting. The interaction process for lower energetic neutrino is hitting a neutron in a water molecule and changes it to proton when corresponding charged lepton is emitted. This channel is called QE (quasi elastic). For antineutrinos is interaction similar, but it hit a proton and changes it to neutron and emit a corresponding antilepton. Higher energetic neutrino can interact with neutron (or nucleus in general) in a water molecule and change it to another particle (for example $\Delta^+ \rightarrow \pi^+ + n^0$ called CCQE-charged current quasi elastic scattering) and emits corresponding charged lepton. These parent particles has lower speed than phase velocity, thus Cherenkov radiation is not emitted. When neutrino's energy is high enough, e or μ created in interaction is faster than the light in the water and creates a detectable cone of light of Cherenkov radiation. This Cherenkov cone is projected as a ring on the walls of the detector. We are able to determine energy of created charged lepton and with a certain precision a direction of neutrino trajectory. Thanks to the fact, that muon is thousand times heavier, it is possible to distinguish an electron from muon. Muon has sharp edge of the ring, thanks to its straight trajectory, but electron's ring is fuzzy because of not straight movement and secondary particles emitted by ionization.

Successor of Super-K is the Hyper-Kamiokande experiment (Hyper-K) [8], same type (water Cherenkov detector) currently under construction and expected to begin data taking in 2028. It is twenty times larger than Super-K and it will have better performance in direction and energy reconstruction thanks to better PMTs. PMTs will be more sensitive to less-energetic events and will have better time resolution. Hyper-K will measure accelerator neutrinos (it will continue on similar baseline as T2K), atmospheric neutrinos, proton decay (and could increase an estimation its halftime), solar neutrinos and supernova neutrinos.

Focus of this thesis is the oscillation of atmospheric neutrinos, prediction of number of ν interactions measured by the Super-Kamiokande. This text is organised as follows. Section 2 explains basic formalism and theory of neutrino oscillation in vacuum and in matter, in Sec. 3 we go through parameters measurements, most important experiments and principles, how each experiment is functioning. Section 4 describes the method how the prediction of the measured number of events for Hyper-K was made and states the result of the computation.

Chapter 2

Neutrino Oscillation

Section 2 goes through theory and formalism of oscillation in Sec. 2.1, Sec. 2.3 and Sec. 2.4 of neutrino oscillation in vacuum, where will be defined oscillation amplitude, appearance probability and survival probability. Appearance probability $P(\nu_\alpha \rightarrow \nu_\beta)$ is relative number of neutrinos that have different flavour in measured beam than in source beam ($\alpha \neq \beta$ where α, β denotes one of the n flavour) and survival probability $P(\nu_\alpha \rightarrow \nu_\alpha)$ is relative number of neutrinos that did not oscillated to another flavour. In Sec. 2.5 is derived theory of mass effect and method for computation corresponding probabilities. We consider $\hbar, c = 1$ in all derivations.

2.1 General Formalism of Neutrino Mixing

As we discussed in introduction, experimental results showed oscillation. Neutrino flavour states ν_α are not eigenstates of Hamiltonian. Eigenstates of Hamiltonian are called mass states of neutrino, noted as $|\nu_i\rangle$ where $i = 1, \dots, n$ (n denotes number of neutrino in model). We can say, that each flavoured neutrino is a superposition of this mass states. It means that we can define two different bases, first called flavour base and second mass base. Both bases are considered to be unitary (i.e. orthogonal and normalised), to there exist some complex unitary transition matrix between this two bases defined by formulas

$$|\nu_i\rangle = \sum_{\alpha} U_{\alpha i} |\nu_{\alpha}\rangle, \quad |\nu_{\alpha}\rangle = \sum_i U_{\alpha i}^* |\nu_i\rangle \quad (2.1)$$

and called mixing matrix. Unitarity properties can be expressed like

$$\begin{aligned} \langle \nu_i | \nu_j \rangle &= \delta_{ij}, & \langle \nu_{\alpha} | \nu_{\beta} \rangle &= \delta_{\alpha\beta}, \\ \sum_{\alpha} U_{\alpha i} U_{\alpha j}^* &= \delta_{ij}, & \sum_i U_{\alpha i} U_{\beta i}^* &= \delta_{\alpha\beta}. \end{aligned} \quad (2.2)$$

2.2 General Formalism of Neutrino Oscillation

Fact, that flavoured neutrinos are not eigenstates of Hamiltonian means, that we cannot evolve flavour states of neutrino, but states. In vacuum we obtain, according to the free Schrödinger equation, plane wave.

$$|\nu_i(\mathbf{x}, t)\rangle = e^{-ip_i \cdot \Delta x} |\nu_i(\mathbf{x}', t')\rangle = e^{-i(E_i \Delta t - \mathbf{p}_i \cdot \Delta \mathbf{x})} |\nu_i(\mathbf{x}', t')\rangle, \quad (2.3)$$

where $\Delta t := t - t'$, $\Delta \mathbf{x} := \mathbf{x} - \mathbf{x}'$, $p_i = (E_i, \mathbf{p}_i)$ is four-momentum of i -th mass state neutrino, $x = (t, \mathbf{x})$ space-time point where beam is measured, $x' = (t', \mathbf{x}')$ space-time point of source and m_i is mass of each mass state of neutrino. We can see that free neutrino is not changing direction of movement, therefore our coordinate system can be defined into direction of movement in 1 dimensional x axis. Space vectors can be replaced as $\mathbf{x} \rightarrow x$.

Using the fact that neutrino has significantly small mass compared to its energy, it is reasonable to use ultra-relativistic limit ($v \rightarrow c$ and $E_i \gg m_i$).

$$\Delta x \approx \Delta t = L, \quad (2.4)$$

$$p_i = \sqrt{E_i^2 - m_i^2} = E_i \sqrt{1 - \frac{m_i^2}{E_i^2}} \approx E_i - \frac{m_i^2}{2E_i}, \quad (2.5)$$

$$\phi_i := E_i \Delta t - p_i \Delta x \approx \frac{m_i^2 L}{2E_i}, \quad (2.6)$$

where L is distance between two points in space and ϕ_i an evolving phase of plane wave.

When we want to evolve flavour state, we have to change base into mass states using Eq. (2.1), because flavour states are not eigenstates of Hamiltonian, as has been said before. Therefore, flavour states can not be evolved by Eq. (2.3), but like this

$$|\nu_\beta(x, t)\rangle = \sum_i U_{\beta i}^* e^{-i \frac{m_i^2 L}{2E_i}} |\nu_i(x', t')\rangle = \sum_{i, \gamma} U_{\beta i}^* e^{-i \phi_i} U_{\gamma i} |\nu_\gamma(x', t')\rangle \quad (2.7)$$

and finally amplitude matrix can be defined as $A(\nu_\alpha(x', t') \rightarrow \nu_\beta(x, t)) := A_{\beta\alpha}(L)$, so

$$A_{\beta\alpha} = \langle \nu_\beta(x, t) | \nu_\alpha(x', t') \rangle = \sum_{i, \gamma} U_{\beta i} e^{i \phi_i} U_{\gamma i}^* \langle \nu_\gamma(x', t') | \quad (2.8)$$

$$|\nu_\alpha(x', t')\rangle = \sum_{i=1}^n U_{\beta i} e^{i \phi_i} U_{\alpha i}^*.$$

For later use let us derive whole amplitude matrix for propagation of neutrinos computed by more of partial amplitude matrices through different environments. When neutrinos oscillate through two intervals (firstly in vacuum) trivially $L = L' + L''$, we obtain

$$A(\nu_\alpha(x'', t'') \rightarrow \nu_\beta(x, t)) = \langle \nu_\beta(x, t) | \nu_\alpha(x'', t'') \rangle = \langle \nu_\beta(x, t) | \sum_\gamma |\nu_\gamma(x', t')\rangle \quad (2.9)$$

$$\langle \nu_\gamma(x', t') | \nu_\alpha(x'', t'') \rangle = \sum_\gamma A_{\beta\gamma}(L') A_{\gamma\alpha}(L'')$$

and we can simplify this expression as

$$\begin{aligned} \sum_{\gamma, i, j} U_{\gamma i} e^{i \phi_i} U_{\alpha i}^* U_{\beta j} e^{i \phi_j} U_{\gamma j}^* &= \sum_{i, j} \sum_\gamma U_{\gamma i} U_{\gamma j}^* e^{i \phi_i} U_{\alpha i}^* U_{\beta j} e^{i \phi_j} = \sum_{i, j} \delta_{ij} e^{i \phi_i} U_{\alpha i}^* U_{\beta j} e^{i \phi_j} = \\ &= \sum_i U_{\beta i} e^{i(\phi_i + \phi_i')} U_{\alpha i}^*, \end{aligned} \quad (2.10)$$

so we obtained $A_{\beta\alpha}(L)$ as was expected. We will find out later that oscillation parameters will effectively depend on material, where neutrino propagates and in this case Eq. (2.9) will be important.

Oscillation probability is defined as squared absolute value of amplitude. We can derive general formula for computing probability as

$$\begin{aligned} P(\nu_\alpha \rightarrow \nu_\beta) &:= |A(\nu_\alpha \rightarrow \nu_\beta)|^2 = |A_{\beta\alpha}|^2 = \sum_{i=1}^n U_{\beta i} e^{i\phi_i} U_{\alpha i}^* \sum_{j=1}^n U_{\beta j}^* e^{-i\phi_j} U_{\alpha j} = \\ &= \sum_{i,j} U_{\beta i} U_{\alpha i}^* U_{\beta j}^* U_{\alpha j} e^{i(\phi_i - \phi_j)}. \end{aligned} \quad (2.11)$$

We can modify the difference of phases by another more tricky approximation. We will suppose that mass states was created with same energy or momentum. Therefore, difference of the phases defined in Eq. (2.5) can be simplified as follows

$$\phi_i - \phi_j = \frac{m_i^2 L}{2E_i} - \frac{m_j^2 L}{2E_j} = \frac{\Delta m_{ij}^2}{2E} L, \quad (2.12)$$

where $\Delta m_{ij}^2 := m_i^2 - m_j^2$ is the well-known squared mass difference. We can continue with modification of probability using this approximation as

$$\begin{aligned} P(\nu_\alpha \rightarrow \nu_\beta) &= \sum_{i=j} U_{\alpha i}^* U_{\alpha j} U_{\beta i} U_{\beta j}^* + \sum_{i \neq j} U_{\alpha i}^* U_{\alpha j} U_{\beta i} U_{\beta j}^* e^{i \frac{\Delta m_{ij}^2}{2E} L} = \sum_{i=j} U_{\alpha i}^* U_{\alpha j} U_{\beta i} U_{\beta j}^* + \\ &+ \sum_{i \neq j} U_{\alpha i}^* U_{\alpha j} U_{\beta i} U_{\beta j}^* - 2 \sum_{i \neq j} U_{\alpha i}^* U_{\alpha j} U_{\beta i} U_{\beta j}^* \sin^2 \left(\frac{\Delta m_{ij}^2 L}{4E} \right) + i \sum_{i \neq j} U_{\alpha i}^* U_{\alpha j} U_{\beta i} U_{\beta j}^* \\ &\sin \left(\frac{\Delta m_{ij}^2 L}{2E} \right) = \sum_{i,j} U_{\alpha i}^* U_{\alpha j} U_{\beta i} U_{\beta j}^* - 2 \sum_{i \neq j} U_{\alpha i}^* U_{\alpha j} U_{\beta i} U_{\beta j}^* \sin^2 \left(\frac{\Delta m_{ij}^2 L}{4E} \right) + \\ &+ i \sum_{i \neq j} U_{\alpha i}^* U_{\alpha j} U_{\beta i} U_{\beta j}^* \sin \left(\frac{\Delta m_{ij}^2 L}{2E} \right), \end{aligned} \quad (2.13)$$

where the first term can be simplified as

$$\sum_{i,j} U_{\alpha i}^* U_{\alpha j} U_{\beta i} U_{\beta j}^* = \left(\sum_i U_{\alpha i}^* U_{\beta i} \right) \left(\sum_j U_{\alpha j} U_{\beta j}^* \right) = \left| \sum_i U_{\alpha i}^* U_{\beta i} \right|^2 = \delta_{\alpha\beta}, \quad (2.14)$$

from unitarity of U-matrix, second term

$$\begin{aligned} -2 \sum_{i \neq j} U_{\alpha i}^* U_{\alpha j} U_{\beta i} U_{\beta j}^* \sin^2 \left(\frac{\Delta m_{ij}^2 L}{4E} \right) &= -2 \left(\sum_{i > j} U_{\alpha i}^* U_{\alpha j} U_{\beta i} U_{\beta j}^* \sin^2 \left(\frac{\Delta m_{ij}^2 L}{4E} \right) + \right. \\ &\left. + \sum_{i < j} U_{\alpha i}^* U_{\alpha j} U_{\beta i} U_{\beta j}^* \sin^2 \left(\frac{\Delta m_{ij}^2 L}{4E} \right) \right) = -4 \sum_{i > j} \Re \left(U_{\alpha i}^* U_{\alpha j} U_{\beta i} U_{\beta j}^* \right) \sin^2 \left(\frac{\Delta m_{ij}^2 L}{4E} \right) \end{aligned} \quad (2.15)$$

and last term

$$\begin{aligned}
& i \left(\sum_{i < j} U_{\alpha i}^* U_{\alpha j} U_{\beta i} U_{\beta j}^* \sin \left(\frac{\Delta m_{ij}^2 L}{2E} \right) + \sum_{i > j} U_{\alpha i}^* U_{\alpha j} U_{\beta i} U_{\beta j}^* \sin \left(\frac{\Delta m_{ij}^2 L}{2E} \right) \right) = \\
& = i \sum_{i > j} \left(U_{\alpha i}^* U_{\alpha j} U_{\beta i} U_{\beta j}^* \sin \left(\frac{\Delta m_{ij}^2 L}{2E} \right) + \left(U_{\alpha i}^* U_{\alpha j} U_{\beta i} U_{\beta j}^* \right)^* \sin \left(-\frac{\Delta m_{ij}^2 L}{2E} \right) \right) = \\
& = -2 \sum_{i > j} \Im \left(U_{\alpha i}^* U_{\alpha j} U_{\beta i} U_{\beta j}^* \right) \sin \left(\frac{\Delta m_{ij}^2 L}{2E} \right). \tag{2.16}
\end{aligned}$$

We obtain general oscillation probability as

$$\begin{aligned}
P(\nu_\alpha \rightarrow \nu_\beta) &= \delta_{\alpha\beta} - 4 \sum_{i > j} \Re \left(U_{\alpha i}^* U_{\alpha j} U_{\beta i} U_{\beta j}^* \right) \sin^2 \left(\frac{\Delta m_{ij}^2 L}{4E} \right) - \\
& \quad - 2 \sum_{i > j} \Im \left(U_{\alpha i}^* U_{\alpha j} U_{\beta i} U_{\beta j}^* \right) \sin \left(\frac{\Delta m_{ij}^2 L}{2E} \right), \tag{2.17}
\end{aligned}$$

for α, β as arbitrary flavour.

2.3 Two-neutrino Oscillation in Vacuum

In two-neutrino framework of oscillation in vacuum we define U 2 by 2 mixing matrix from flavour ($|\nu_\alpha\rangle$ for $\alpha = e$ or x) base to mass base ($|\nu_i\rangle$ for $i = 1, 2$) and can be parameterized by one parameter marked below as θ called mixing angle.

$$U := \begin{pmatrix} \cos \theta & \sin \theta \\ -\sin \theta & \cos \theta \end{pmatrix}. \tag{2.18}$$

For two-neutrino approximation, we use Eq. (2.17) and we simplify with $n = 2$ trivially as

$$P(\nu_\alpha \rightarrow \nu_\beta) = \sin^2(2\theta) \sin^2 \frac{\Delta m^2 L}{4E}, \tag{2.19}$$

where $\alpha \neq \beta$ and the difference of squared masses was denoted as $\Delta m^2 = m_2^2 - m_1^2$. If we plug in remaining c and \hbar , result formula will be

$$P(\nu_\alpha \rightarrow \nu_\beta) \doteq \sin^2(2\theta) \sin^2 \left(1.27 \frac{\Delta m^2 [\text{eV}^2] L [\text{km}]}{E [\text{GeV}]} \right). \tag{2.20}$$

In the case of calculating survival probability $P(\nu_\alpha \rightarrow \nu_\alpha)$, its derivation is pretty similar.

$$P(\nu_\alpha \rightarrow \nu_\alpha) = 1 - \sin^2 2\theta \sin^2 \frac{\Delta m^2 L}{4E}. \tag{2.21}$$

2.4 Three-neutrino Oscillation in Vacuum

For three-neutrino framework we have same formulas for U-matrix, and obviously $n = 3$. Flavours of neutrino are denoted as $\alpha = e, \mu$ and τ . U-matrix

is 3 by 3 and is called PMNS matrix (after pioneers of ν oscillation Pontecorvo, Maki, Nakagawa, Sakata). U-matrix is still unitary (which means that 18 free real parameters, but 9 conditions for unitarity, and 3 parameters are absorbed as phases of the lepton fields) with 6 real parameters. Usually, U-mixing matrix is parameterized in the shape as

$$\begin{aligned}
U &= \begin{pmatrix} U_{e1} & U_{e2} & U_{e3} \\ U_{\mu1} & U_{\mu2} & U_{\mu3} \\ U_{\tau1} & U_{\tau2} & U_{\tau3} \end{pmatrix} = \begin{pmatrix} 1 & 0 & 0 \\ 0 & \cos \theta_{23} & \sin \theta_{23} \\ 0 & -\sin \theta_{23} & \cos \theta_{23} \end{pmatrix} \begin{pmatrix} \cos \theta_{13} & 0 & e^{-i\delta_{CP}} \sin \theta_{13} \\ 0 & 1 & 0 \\ -e^{i\delta_{CP}} \sin \theta_{13} & 0 & \cos \theta_{13} \end{pmatrix} \\
&= \begin{pmatrix} \cos \theta_{12} & \sin \theta_{12} & 0 \\ -\sin \theta_{12} & \cos \theta_{12} & 0 \\ 0 & 0 & 1 \end{pmatrix} \begin{pmatrix} 1 & 0 & 0 \\ 0 & e^{i\alpha_1} & 0 \\ 0 & 0 & e^{i\alpha_2} \end{pmatrix} = \\
&= \begin{pmatrix} c_{12}c_{13} & s_{12}c_{13} & s_{13}e^{-i\delta_{CP}} \\ -s_{12}c_{23} - c_{12}s_{23}s_{13}e^{i\delta_{CP}} & c_{12}c_{23} - s_{12}s_{13}s_{23}e^{i\delta_{CP}} & c_{13}s_{23} \\ s_{12}s_{23} - c_{12}s_{13}c_{23}e^{i\delta_{CP}} & -c_{12}s_{23} - s_{12}s_{13}c_{23}e^{i\delta_{CP}} & c_{13}c_{23} \end{pmatrix} \begin{pmatrix} 1 & 0 & 0 \\ 0 & e^{i\alpha_1} & 0 \\ 0 & 0 & e^{i\alpha_2} \end{pmatrix}, \tag{2.22}
\end{aligned}$$

where θ_{ij} are mixing angles, s_{ij} and c_{ij} is here defined as $s_{ij} := \sin \theta_{ij}$ and $c_{12} := \cos \theta_{12}$. For oscillation other parameters are important such as Δm_{ij}^2 as it can be seen in Eq. (2.17), but by definition we need only two independent parameters in three neutrino framework, because $\Delta m_{21}^2 + \Delta m_{32}^2 = \Delta m_{31}^2$. For normal mass hierarchy, Δm_{21}^2 and Δm_{32}^2 are positive numbers. Δm_{31}^2 parameter is used for so called inverted hierarchy and is negative.

Parameter	Global fit value
$\sin^2(\theta_{12})$	0.307 ± 0.013
$\sin^2(\theta_{23})$	0.546 ± 0.021
$\sin^2(\theta_{13})$	$(2.20 \pm 0.07) \times 10^{-2}$
Δm_{21}^2	$(7.53 \pm 0.18) \times 10^{-5} \text{ eV}^2$
Δm_{32}^2	$(2.453 \pm 0.033) \times 10^{-3} \text{ eV}^2$
δ_{CP}	$(1.23 \pm 0.21) \pi \text{ rad}$

Table 2.1: Measured values of parameters of neutrino oscillations in normal order taken from PDG with $\pm 1\sigma$ [9].

Most of these parameters are known and measured values can be found in Tab. 2.1. The remaining parameters α_1 and α_2 are Majorana phases, which takes no role in oscillations and was not established or measured. δ_{CP} is phase of CP (charge-parity) violation and is measured by comparing of antineutrinos and neutrinos oscillation (to be more specific, $P(\nu_\mu \rightarrow \nu_e) \neq P(\bar{\nu}_e \rightarrow \bar{\nu}_\mu)$). Experiment NO ν A and T2K showed some indications of CP violation, but there is still no clear evidence.

To determine oscillation parameters, you need to know the oscillation probability. Definition is same as in Eq. (2.11), but, unfortunately, the probability can not be reasonably simplified in this case, so Eq. (2.17) will be used in its form. We can see that third term of Eq. (2.17) is nonzero if and only if $\delta_{CP} \neq 0, \pi$ in three-neutrino framework. In two neutrino framework, there is not enough free parameters in U-mixing matrix thus it is not possible to include CP violation in U parametrization in this framework.

2.5 Matter Effect

We calculated, how neutrinos oscillate when propagate in vacuum. Neutrino oscillation through matter is different because of presence of e^- . This phenomenon is called matter effect. As was told before, mass state of neutrino is eigenvalue of Hamiltonian. It can be expressed in two-neutrino approximation as

$$\begin{aligned} i\frac{d}{dt}\begin{pmatrix} |\nu_1\rangle \\ |\nu_2\rangle \end{pmatrix} &= \hat{H}\begin{pmatrix} |\nu_1\rangle \\ |\nu_2\rangle \end{pmatrix}, \text{ where } H = \begin{pmatrix} E_1 & 0 \\ 0 & E_2 \end{pmatrix} \approx E\mathbb{I} + \frac{1}{2E}\begin{pmatrix} m_1^2 & 0 \\ 0 & m_2^2 \end{pmatrix} \\ &= \left(E + \frac{m_1^2}{2E}\right)\mathbb{I} + \frac{1}{2E}\begin{pmatrix} 0 & 0 \\ 0 & \Delta m_{21}^2 \end{pmatrix} \end{aligned} \quad (2.23)$$

and we can evolve flavour states as

$$i\frac{d}{dt}\begin{pmatrix} |\nu_e\rangle \\ |\nu_\mu\rangle \end{pmatrix} = iU^\dagger\frac{d}{dt}\begin{pmatrix} |\nu_1\rangle \\ |\nu_2\rangle \end{pmatrix} = U^\dagger\hat{H}\begin{pmatrix} |\nu_1\rangle \\ |\nu_2\rangle \end{pmatrix} = U^\dagger\hat{H}U\begin{pmatrix} |\nu_e\rangle \\ |\nu_\mu\rangle \end{pmatrix}. \quad (2.24)$$

In matter we can suppose that neutrino is feeling a coherent forward scattering potential V_α . This potential is weak interaction between neutrino and electron in matter. Coherent forward scattering means that phase of neutrino is not interrupted by interaction and also direction of neutrino movement is not changed as much as neutrino would not be detected.

Weak interaction has two possibilities called neutral and charged channel. As you could think, this two channels are distinguished by intermediate particle in interaction. In charged channel is intermediate particle W^\pm boson and in neutral channel Z^0 boson. Only electron neutrino can interact with electron through charged channel because of lepton number conservation. With both currents is electron neutrino, ν_μ is interacting only by neutral current. This difference of interaction is used as follows

$$\begin{aligned} i\frac{d}{dt}\begin{pmatrix} |\nu_e\rangle \\ |\nu_\mu\rangle \end{pmatrix} &= (U^\dagger\hat{H}U + V)\begin{pmatrix} |\nu_e\rangle \\ |\nu_\mu\rangle \end{pmatrix} = \left[U^\dagger\left(E + \frac{m_1^2}{2E}\right)\mathbb{I}U + U^\dagger\frac{1}{2E}\begin{pmatrix} 0 & 0 \\ 0 & \Delta m_{21}^2 \end{pmatrix}U + \begin{pmatrix} V_e & 0 \\ 0 & V_\mu \end{pmatrix}\right]\begin{pmatrix} |\nu_e\rangle \\ |\nu_\mu\rangle \end{pmatrix} \\ &= \left[\left(E + \frac{m_2^2}{2E} + V_\mu\right)\mathbb{I} + U^\dagger\frac{1}{2E}\begin{pmatrix} 0 & 0 \\ 0 & \Delta m_{21}^2 \end{pmatrix}U + \begin{pmatrix} \Delta V & 0 \\ 0 & 0 \end{pmatrix}\right]\begin{pmatrix} |\nu_e\rangle \\ |\nu_\mu\rangle \end{pmatrix} \\ &= \left[H_0 + \begin{pmatrix} \sin^2\theta\frac{\Delta m_{21}^2}{2E} + \Delta V & -\sin\theta\cos\theta\frac{\Delta m_{21}^2}{2E} \\ -\sin\theta\cos\theta\frac{\Delta m_{21}^2}{2E} & \cos^2\theta\frac{\Delta m_{21}^2}{2E} \end{pmatrix}\right]\begin{pmatrix} |\nu_e\rangle \\ |\nu_\mu\rangle \end{pmatrix}, \end{aligned} \quad (2.25)$$

where $\Delta V = 2\sqrt{2}G_F EN_e$ is above-mentioned difference of interaction, $G_F = 1.166 \times 10^{-5} \text{ GeV}^{-2}$ called Fermi constant, E energy of neutrino and N_e density of electrons in matter. We can neglect $H_0 = \left(E + \frac{m_2^2}{2E} + V_\mu\right)\mathbb{I}$, the part of the Hamiltonian which is just proportional to identity matrix, thus play no role in oscillation. This non-diagonal Hamiltonian can be diagonalized to the shape similar to free Hamiltonian as

$$i\frac{d}{dt}\begin{pmatrix} |\nu_e\rangle \\ |\nu_\mu\rangle \end{pmatrix} = U_m^\dagger\begin{pmatrix} m_{1m}^2 & 0 \\ 0 & m_{2m}^2 \end{pmatrix}U_m\begin{pmatrix} |\nu_e\rangle \\ |\nu_\mu\rangle \end{pmatrix}, \quad (2.26)$$

where m_{1m}^2 are eigenvalues of matrix Eq. (2.25) denoted as effective masses of mass states in matter. U_m is transition matrix to the base, where matrix is diagonal. U_m is unitary matrix and can be parameterized as U-matrix with effective mixing angle denoted as θ_m . For two-neutrino framework can be this diagonalization done explicitly, but it will not be used in text. For more dimensions of matrices (more neutrino frameworks) can be done numerical computation, or others approximations. Our hardly earned modified parameters m_{im} and θ_{ijm} can be used in Eq. (2.17), Eq. (2.20) and also in Eq. (2.8) to express probabilities of oscillations in matter.

Chapter 3

Neutrino Sources and Measurement

Neutrinos are created in weak interactions. That means, they can be created anywhere by beta decay of atom nuclei. Different sources require different types of experiments and different mechanisms of neutrino detection.

As it can be seen in formula Eq. (2.17) and from parameterization of U mixing matrix in three neutrino framework from Eq. (2.22), the most of parameters, which the oscillation depends on, has been measured. Mechanisms and experiments leading to the knowledge of various aspects of neutrino physics are discussed in following text.

3.1 The θ_{12} and Δm_{21}^2 Measurement

The biggest natural neutrino source near us is the Sun. To create one nucleus of relatively stable helium three ($T_{\frac{1}{2}} \approx 12$ y) is one neutron needed for fusion of hydrogen and deuterium. Neutron is created by β^+ conversion. One example of β^+ conversion is described by following equation $p^+ + p^+ \rightarrow {}^2\text{H} + e^+ + \nu_e$. Only electron neutrinos can be created by these processes, because there is not enough energy to create μ^+ . Neutrinos created in this exact reaction are called pp neutrinos and typically has energies below 0.4 MeV. While pp ν make up approximately 91 % of solar neutrinos, in the Fig. 3.1 are shown different neutrinos producing processes like pep ν , ${}^7\text{Be}$ or ${}^8\text{B}$ ν created in similar reactions like pp ν . Different experiments with various detection techniques are sensitive to different parts of this energy spectrum.

The Homestake experiment was one of the first experiment measuring solar neutrinos, as it was said before. This experiment took data until 1994 and worked on the principle of $\nu_e + {}^{37}\text{Cl} \rightarrow {}^{37}\text{Ar} + e^-$ conversion with a threshold of 0.81 MeV. There was used 380 m³ of perchloroethylene as a source of chlorine and ${}^{37}\text{Ar}$ was chemically extracted and determined its amount. Number of ν_e interactions was gained from amount of the obtained argon.

Other experiments can be mentioned for completeness, such as the Borexino experiment and the SNO experiment. The Borexino [11] (Boron solar neutrino Experiment, smaller than original proposal BOREX) was taking data until 2021 and it is decommissioned now. The Borexino was a spherically shaped calorimeter with inward facing PMTs. In this experiment a neutrino collides with an electron

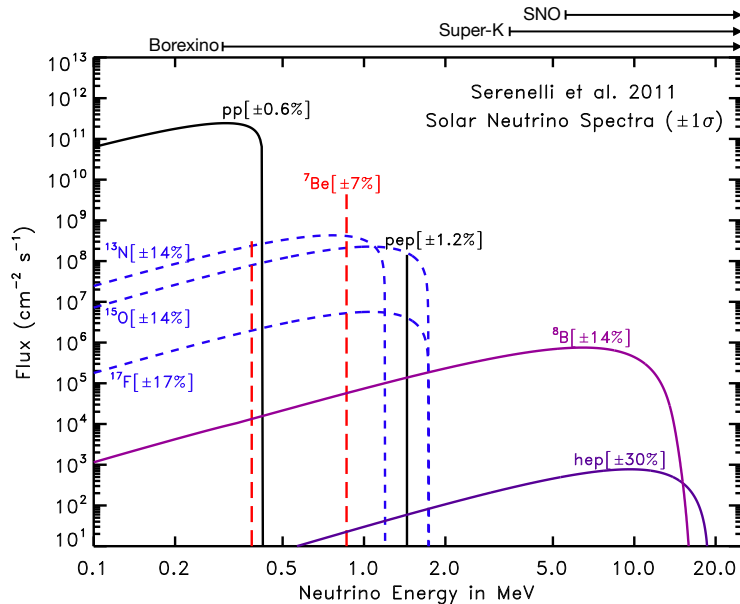


Figure 3.1: The Standard Solar Model prediction of solar neutrino flux from various creation processes [10]. Thresholds of some solar neutrino experiments are indicated at the top of the graph.

that is stopped in scintillator while light is produced. The experiment was able to detect all individual fluxes separately, or more precisely could indicate more neutrino types created in the Sun in different processes. Energy of neutrino can be determined from the number of emitted photoelectrons on PMTs. The Borexino measured mainly solar neutrinos (pp, or CNO ν), but they were able to detect even geo-neutrinos.

Possible explanation of the Solar Neutrino Problem was the MSW effect and to resonances of the oscillation parameters in matter (will be discussed in the Sec. 4.2) and allow us to measure θ_{12} sometimes called the solar mixing angle. This resonance causes transition in ν_{2m} state in resonance density as is described here [12]. That means probability of measuring ν_e is in ideal case

$$P(\nu_{2m} \rightarrow \nu_e) = \sin^2 \theta_{12}. \quad (3.1)$$

Experimental result (more precisely, the global fit value of various experiments) of measuring this parameter can be found in Tab. 2.1.

Although, parameter Δm_{21}^2 can be measured from solar neutrinos, too (using little more complicated fit of probability), the most precise results was gained by the KamLAND experiment (Kamioka Liquid Scintillator Antineutrino Detector) in Japan measuring reactor neutrinos. The KamLAND experiment [13] is translucent mineral oil liquid scintillator (LS) of spherical shape balloon with 13 m in diameter combined with buffer oil and outer Cherenkov detector with inward-facing PMTs. Liquid scintillator is a neutrino target and it is separated from the buffer oil by transparent Nylon foil. The buffer oil is transparent for photons created in the LS and is used as a shield of outer gamma photons (and from PMTs) and for carrying weight of the balloon. This inner part of detector is enclosed in stainless steel spherical vessel with a diameter of 18 m, which optically separate the inner and outer parts. The outer Cherenkov detector has function

of cosmic ray anti-counter usually called μ veto detector. The experiment was mainly constructed for detecting reactor $\bar{\nu}_e$ from more than 50 nuclear reactors.

Detection principle is inverse β transition of free proton $\bar{\nu}_e + p^+ \rightarrow e^+ + n^0$ at inner scintillator part with minimum energy of neutrino required for this reaction is 1.8 MeV. Created e^+ emits light and annihilation γ 's, n^0 is thermalised by colliding with protons and can be absorbed by hydrogen nucleus emitting characteristic 2.2 MeV γ -ray signal by process $^1\text{H} + n^0 = ^2\text{H} + \gamma$. This delayed signal of neutron absorption has mean capture time approximately 200 μs .

The KamLAND performed much better measurement of the Δm_{21}^2 parameter, than latter experiments from measuring Sun ν , and they were able to determine the θ_{12} mixing angle, too.

Moreover, the KamLAND experiment (to be more specific, its upgrade called the KamLAND-Zen experiment [14]) searches for so-called neutrinoless double beta decay and the experiment is able to measure even geo-neutrinos created in natural heavy nuclei.

3.2 The θ_{23} and Δm_{32}^2 Measurement

Parameters θ_{23} and Δm_{32}^2 were measured in the atmospheric neutrino detectors for the first time. First indication of $\nu_\mu \rightarrow \nu_\tau$ oscillation was measured at the Super-K by observing ν_μ disappearance. Results showed the difference of the ν_μ fluxes from above and from below the horizon, what could mean that neutrinos oscillated after travel whole way through the Earth [15]. But, the ν_e number of events (left part of Fig. 3.2) did not change from the prediction, what means that some ν_μ particles oscillated to ν_τ neutrinos (supposing three neutrino framework). Also, this measured difference depends on energy (at the figure from top to bottom) and where can be seen certain decrease of measured number of events compared to the non-oscillated predicted number of events. The interpretation of this reduction is $\nu_\mu \rightarrow \nu_\tau$ oscillation. The ν_τ can not be identified directly in the Super-K due to short lifetime of a τ^- particle ($T_{\frac{1}{2}} = 2.9 \times 10^{-13}$ s compared to μ^- $T_{\frac{1}{2}} = 2.2 \times 10^{-6}$ s [9])

The Super-K experiment is a water Cherenkov detector near the Kamioka town in Japan. It was constructed as successor of the KamiokaNDE experiment and its original purpose is to search for the proton decay (and bring lower bound to $T_{\frac{1}{2}} = 1.67 \times 10^{34}$ y [15]).

Other measurement of atmospheric neutrinos are at the ANTARES telescope in the Mediterranean Sea [16] and the IceCube experiment [17] constructed at the Amundsen-Scott South Pole Station. The IceCube experiment is specialised for measuring cosmic neutrinos from outer space and it is sensible for high energetic neutrinos (in the range of 10 GeV - 100 TeV).

Parameters θ_{23} and Δm_{23}^2 can be determined by measuring the probability

$$P(\nu_\mu \rightarrow \nu_\mu) \simeq 1 - \sin^2 2\theta_{23} \sin^2 \frac{\Delta m_{32}^2 L}{4E} \quad (3.2)$$

from Eq. (2.17) which was simplified using $|\Delta m_{21}^2| \ll |\Delta m_{31}^2|$ and $\cos^2 \theta_{13} \rightarrow 1$.

Experiments measuring accelerator neutrinos, are the T2K experiment [5] and the NO ν A experiment [18] measuring ν_μ disappearance corresponding to θ_{23}

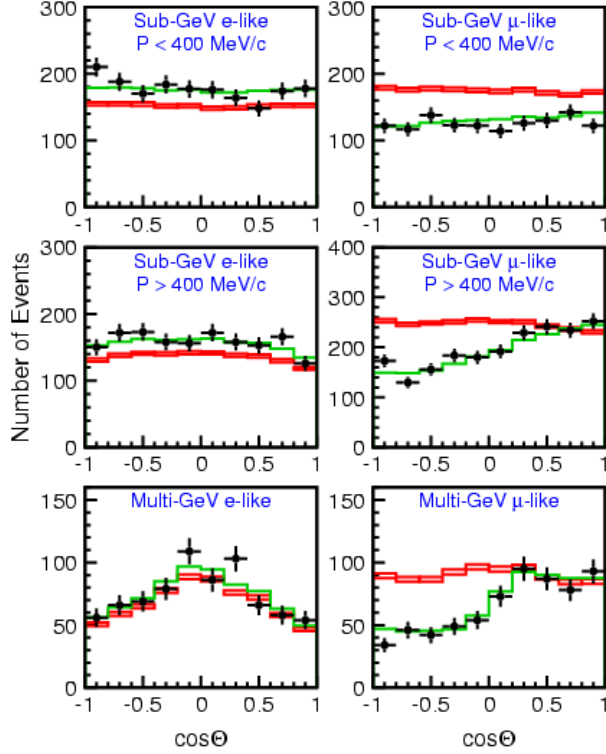


Figure 3.2: Measured cosine zenith angle distributions of fluxes measured by Super-K for e-like (left) and μ -like (right) neutrinos in three energetic regions, i.e. lower than 0.4 GeV, from 0.4 GeV to 1.4 GeV and above 1.4 GeV (multi-GeV) [15].

mixing angle. The T2K experiment detects accelerator neutrino beam created in the J-PARC facility near the Tokai village in Japan. The NO ν A experiment measures accelerator neutrinos created in the Fermilab particle accelerator in USA near Chicago. The neutrino beam is created in experiment called NuMI (Neutrino at the Main Injector) and, similarly for both experiments, proton bunch is directed to an immediate target placed, where mainly pions and kaons are created. These mesons are separated by the type of particles, which are required for the neutrino beam creation (there can be chosen π^+ resp. π^- for ν_μ resp. $\bar{\nu}_\mu$) and they are focused to the beam by magnetic horns. The separated particle beam is send to the decay pipe, where mesons decay to the ν_μ and μ . The beam continues through the ground to the experiment supposing, that the ground absorbs almost all μ particles, which are undesirable for neutrino measurement. Almost pure ν_μ beam is created in this process with $< 1\%$ contamination at flux peak energy.

The NO ν A (NuMI Off-Axis ν_e Appearance) [18] experiment is an example of near-far detector, where both detectors are the same design. Both detectors placed approximately 14 mrad (corresponding to 12 km for far detector) off the axis of the NuMI beamline (because of more suitable energy distribution of neutrinos) and are placed 1 km for near detector (ND) and 810 km for far detector (FD) from the NuMI target. The ND is placed at Fermilab, and FD is placed in Minnesota near Ash River.

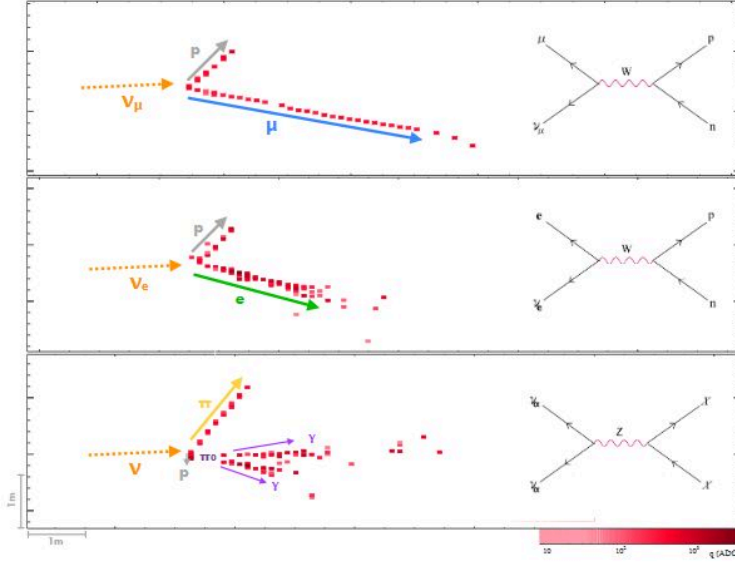


Figure 3.3: Measuring principle used for separating ν_e and ν_μ [19].

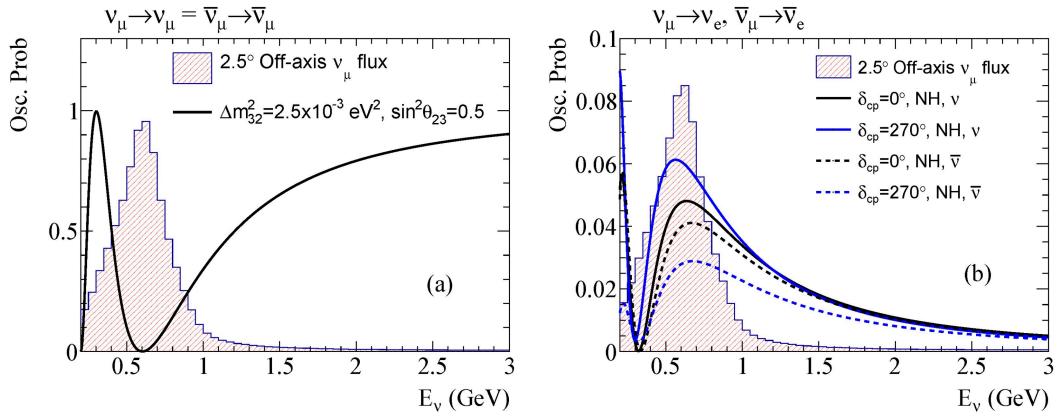


Figure 3.4: Off-axis energy distributions of ν fluxes and corresponding oscillation probabilities of the T2K experiment [20].

The flavour of incoming neutrino is determined by the trajectory of products particles as it can be seen in Fig. 3.3. Interesting fact about the FD, that the detector is placed practically on the surface, although the other experiments (such as the MINOS experiment, the Super-K experiment or the KamLAND experiment) were built underground because of cosmic ray reduction. The NO ν A experiment relies on precise timing and a well-defined beam direction and energy to recognise correct signals in the analysis.

The J-PARC is a complex of particle accelerator creating proton bunch and neutrino beam for Super-K experiment similarly as the NuMI for the NO ν A experiment. Neutrino beam is created using 30 GeV protons. The T2K has also ND (ND280, because of the distance between the target at J-PARC and ND is 280 m) and FD (the Super-K experiment) located 2.5 degrees off the axis, which creates so called narrow-band-neutrino beam with the peak energy around 0.6 GeV as you can see in the Fig. 3.4. The ND does not measure neutrino interactions as the NO ν A ND, but it monitors μ and mesons created by collision

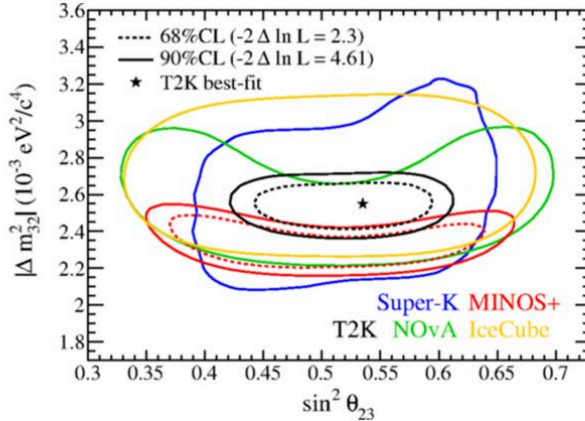


Figure 3.5: Compilation of results of $\sin^2 \theta_{23}$ and $|\Delta m_{32}^2|$ parameters fits for different experiments from 2017 [21].

in the target. The Super-K is located at 295 km long base line and measures neutrino fluxes. This setup ($E_\nu \approx 0.6$ GeV, $L_\nu = 295$ km) nicely corresponds to the first oscillation minimum as can be seen in Fig. 3.4, too.

Systematic errors of the T2K experiment were estimated such low, that approximations mentioned earlier played a role in the measurement. The result of θ_{23} and Δm_{32}^2 parameters fitted for T2K experiment compared to other experiments (such as the NO ν A, MINOS+ or IceCube experiment) can be seen in Fig. 3.5 where can be spotted slightly better relative precision with determination of Δm_{32}^2 parameter compared to relative precision of $\sin^2 \theta_{23}$ measurement.

3.3 The θ_{13} and Δm_{31}^2 Measurement

As has been said in the introduction, an important source of antineutrinos are nuclear reactors. Heavy elements nuclei (mainly ^{235}U) are split to more so called daughter nuclei and some thermal neutrons. These daughter nuclei have neutron proton ratio higher than is required for stable nucleus (so called neutron-rich) thus are unstable. Hence, these isotopes (or fission products) decay to more stable nuclei by cascade of β^- decays with emission of $\bar{\nu}_e$ s. Number of created neutrinos depends on the size, or thermal power of nuclear reactor, but we can estimate, that approximately 2×10^{20} $\bar{\nu}_e$ antiparticles are created per second per gigawatt of produced thermal power (/s/GW_{th}). This number makes every nuclear plant a strong source of electron antineutrinos (compared to the flux from other sources of antineutrinos).

Parameters θ_{13} and Δm_{31}^2 are determined by measuring survival probability of electron antineutrinos. Formula can be obtained from Eq. (2.17) and can be simplified to the expression

$$\begin{aligned}
 P(\bar{\nu}_e \rightarrow \bar{\nu}_e) = & 1 - \cos^4 \theta_{13} \sin^2 \theta_{12} \sin^2 \left(\frac{\Delta m_{21}^2 L}{4E} \right) - \\
 & - \sin^2 2\theta_{13} \left(\cos^2 \theta_{12} \sin^2 \left(\frac{\Delta m_{31}^2 L}{4E} \right) - \sin^2 \theta_{12} \sin^2 \left(\frac{\Delta m_{32}^2 L}{4E} \right) \right).
 \end{aligned}
 \tag{3.3}$$

The last term is usually parametrized with Δm_{ee}^2 and by defining single effective disappearance phase, so result formula can be written as

$$P(\bar{\nu}_e \rightarrow \bar{\nu}_e) = 1 - \cos^4 \theta_{13} \sin^2 \theta_{12} \sin^2 \left(\frac{\Delta m_{21}^2 L}{4E} \right) - \sin^2 2\theta_{13} \sin^2 \left(\frac{\Delta m_{ee}^2 L}{4E} \right). \quad (3.4)$$

An important experiment measuring reactor antineutrinos was the Daya Bay experiment, which stopped taking data recently at 2020 [22, 23]. The main goal of the Daya Bay measurement was a proof of nonzero value of the θ_{13} parameter. The Daya Bay experiment was liquid gadolinium-doped scintillator detector in China and it is able to measure $\sin^2(2\theta_{13})$ and Δm_{31}^2 . Detection principle is similar for every other experiment measuring reactor neutrinos (such as KamLAND, RENO, future JUNO or Double Chooz) described by formula $\bar{\nu}_e + p^+ \rightarrow e^+ + n^0$ mentioned earlier. Whole experiment was composed of functionally identical cylindrical antineutrino detectors, each containing 20 tons of scintillator used as active target for neutrinos and inward facing PMTs. Whole gadolinium-doped scintillator is surrounded by γ catcher and water veto system with PMTs. The non-scintillating liquid buffer is placed between γ catcher and veto system to minimize the external radiation mainly from PMTs, but the secondary radiation made by cosmic μ 's, too.

There were used eight functionally identical detectors, four tanks were used as near detectors ($L_n \approx 500$ m) placed in pairs in EH1 and EH2 (abbreviation for Experimental Hall) and rest four tanks as far detectors placed in EH3 and suited in first oscillation minimum ($L_f \approx 1.6$ km). This near-far detector arrangement was essential to overcome uncertainty in the $\bar{\nu}_e$ flux from source, hence the Daya Bay experiment was able to measure oscillation parameters more precisely than previous single detector experiments (the KamLAND experiment, etc.).

The Daya Bay experiment measured combined flux of antineutrinos created in the Daya Bay and the Ling Ao nuclear power plants in six nuclear reactors each with thermal power of 2.9 GW_{th}. Nuclear reactors are arranged in two so called clusters, two reactors by the EH1 and four by the EH2. The EH3 is buried under mountains next to the nuclear plant, which provide certain shield against atmospheric muons. EH1 and EH2 are also underground, but with less overburden.

The general detection principle was described earlier. Positron created by collision of antineutrino and proton present in the scintillator is ionizing and emits photons. A neutron is simultaneously created with positron in the neutrino collision, it is thermalised and after some time is captured on a gadolinium nucleus and rapidly de-excites by emitting 3-4 characteristic γ -ray with the total energy of 8 MeV photons with mean delay time around 30 μ s. This neutron γ -ray photons help us with resolution between $\bar{\nu}_e$ interactions from background. Inward facing PMTs allow only calorimetric measurement, therefore no information about the direction of original antineutrino is available. The antineutrino energy is calculated using measured $E_{prompt} \simeq T_{e^+} + 2m_e$ and basic kinematics of inverse β decay as $E_\nu \simeq E_{prompt} + 0.8$ MeV. Parameters are gained by fit of measured data shown at Fig. 3.6 and the results are really close to the values at Tab. 2.1

as the Daya Bay experiment was the most precise experiment ever measuring the θ_{13} parameter.

Other experiment that measures reactor antineutrinos is RENO (Reactor experiment for neutrino oscillation) by the Yonggwang nuclear power plant in Korea. The Yonggwang power plant is composed from six reactors placed in equally spaced span in line. The distance of two neighbor reactors is roughly 1280 m and thermal power of the whole Yonggwang power plant is 16.4 GW_{th} (a bit lower than the Ling Ao power plant with roughly 17.4 GW).

RENO [24] is another example of the near-far detector similarly as the Daya Bay. Its main goal is the $\sin^2 2\theta_{13}$ measurement. The experiment also confirmed the Daya Bay experiment result, that $\sin^2 2\theta_{13} \neq 0$. Unlike the Daya Bay experiment, RENO has two identically designed 16.5 t gadolinium-doped liquid scintillator detectors placed 294 m and 1383 m from the center of the reactor array. As usual, detectors are placed underground because of atmospheric muons shielding (can be expressed as 120 m for ND and 450 m for FD of water-equivalent rock overburden). Identically designed detectors bring advantages like to cancel out the systematic uncertainties of comparison of non-oscillated and oscillated fluxes from near and far detector.

As has been said earlier, the French Double Chooz [25] experiment was measuring reactor antineutrinos and θ_{13} and Δm_{31}^2 parameters, too. The Double Chooz experiment is another example of gadolinium-doped near-far detector with two identical detectors and was able to bring limits for $\sin^2 2\theta_{13}$ angle and they confirmed nonzero value of $\sin^2 2\theta_{13}$ angle as well.

JUNO [26] (Jiangmen Underground Neutrino Observatory) is multipurpose experiment and it will measure also reactor neutrinos, but at medium baseline (52.5 km). JUNO should improve the $\sin^2 2\theta_{12}$, Δm_{21}^2 and Δm_{31}^2 uncertainty under 1 %, but it will not measure θ_{13} parameter better than Daya Bay.

Parameters θ_{13} and Δm_{31}^2 can be also measured at accelerator neutrinos, namely at the T2K experiment. Accuracy of this measurement is worse than at reactor neutrinos because of unknown δ_{CP} phase value.

3.4 The δ_{CP} Measurement

The challenging open question for neutrino physics is the δ_{CP} phase determination. The δ_{CP} phase is directly related to so called CP violation and, as it was briefly said in previous text, it expresses the differences between oscillation probability of neutrinos and antineutrinos. Hence, the most suitable way of δ_{CP} determination is measurement of accelerator neutrinos in two phase run, $P(\nu_\mu \rightarrow \nu_e)$ and $P(\bar{\nu}_\mu \rightarrow \bar{\nu}_e)$. As it can be seen in Tab. 2.1, value of the phase is not determined with sufficient statistical significance. Experiments measuring δ_{CP} are the T2K experiment and the NO ν A experiment.

The T2K experiment [5] has been alternating between neutrino and antineutrino configurations since 2014. The results were indicating CP-violation with insufficient statistical significance to prove that. Results plotted on $\sin^2 \theta_{13} - \delta_{CP}$ contour can be seen in the Fig. 3.7. The result and the uncertainty of the determined value depends on measured oscillation parameters and their constraints. The effect of the θ_{13} region is called the reactor constraint and the analysis included the reactor constraint is in the Fig. 3.7.

Another experiment, which measures the δ_{CP} phase, is the NO ν A experiment [18]. However, the NO ν A experiment has basically identical measurement principle for δ_{CP} phase determination, the results almost contradicts with results of the T2K experiment if we would assume the normal ordering as it can be seen in the Fig. 3.8. The result could be consistent for inverted ordering for in 1σ region.

The future experiment set to determine the δ_{CP} parameter much more precisely than the previous experiments is Hyper-Kamiokande [28]. The Hyper-Kamiokande experiment should be able to take off non-negligible region of the δ_{CP} values. It will measure δ_{CP} phase by almost pure accelerator ν_μ (or $\bar{\nu}_\mu$) beam created by J-PARC, same as in the T2K experiment, but upgraded. The number of neutrinos in the beam will be increased by higher total number of protons used per beam and by higher repetition rate of the beams creation as well. The upgrade is said to be stronger from 515 kW (currently used for T2K) to 1.3 MW. The Hyper-K experiment will be composed from three detectors. The near detector will be upgraded ND280 detector, second part will be an one kiloton Intermediate Water Cherenkov Detector (IWCD) built 1 km from the neutrino production target and the Hyper-K itself (with the baseline of 295 km 2.5° off axis, similar to T2K).

The IWCD is proposed to be kiloton-scale water Cherenkov detector and apart from other detectors, it will be able to move vertically to measure the neutrino beam intensity and energy spectrum at different off-axis angles (from 1° to 4°). The main goal of this detector is neutrino cross section measurements (3% for $\frac{\sigma(\nu_e)}{\sigma(\nu_\mu)}$ and 5% for $\frac{\sigma(\bar{\nu}_e)}{\sigma(\bar{\nu}_\mu)}$).

As it can be seen at Tab. 2.1, it is still not clear if CP parity of the neutrino oscillation is violated or conserved.

The next future experiment arranged to measure δ_{CO} is the Deep Underground Neutrino Experiment (DUNE). The experiment will measure accelerator neutrinos, created in the Fermilab particle accelerator (similarly as NO ν A) by so called Long Baseline Neutrino Facility, and it will also measure atmospheric neutrinos with higher energetic resolution for sub-GeV region, than previous experiments. The results will be important in the θ_{23} measurement and δ_{CP} phase at long base line.

The experiment is another example of the near-far detector and it is currently under construction. The near detector will measure neutrinos 600 m from the neutrino-production target by the complicated combination of the three different types of subdetectors (one scintillator tracker and two argon-based). It will be important for making accurate predictions of the fluxes and the cross sections. The far detector will be liquid argon time projection chamber made up of 70 kton liquid argon placed 1.5 km under the surface and 1300 km far from target. But, the measurement of the atmospheric neutrinos will be more important for us.

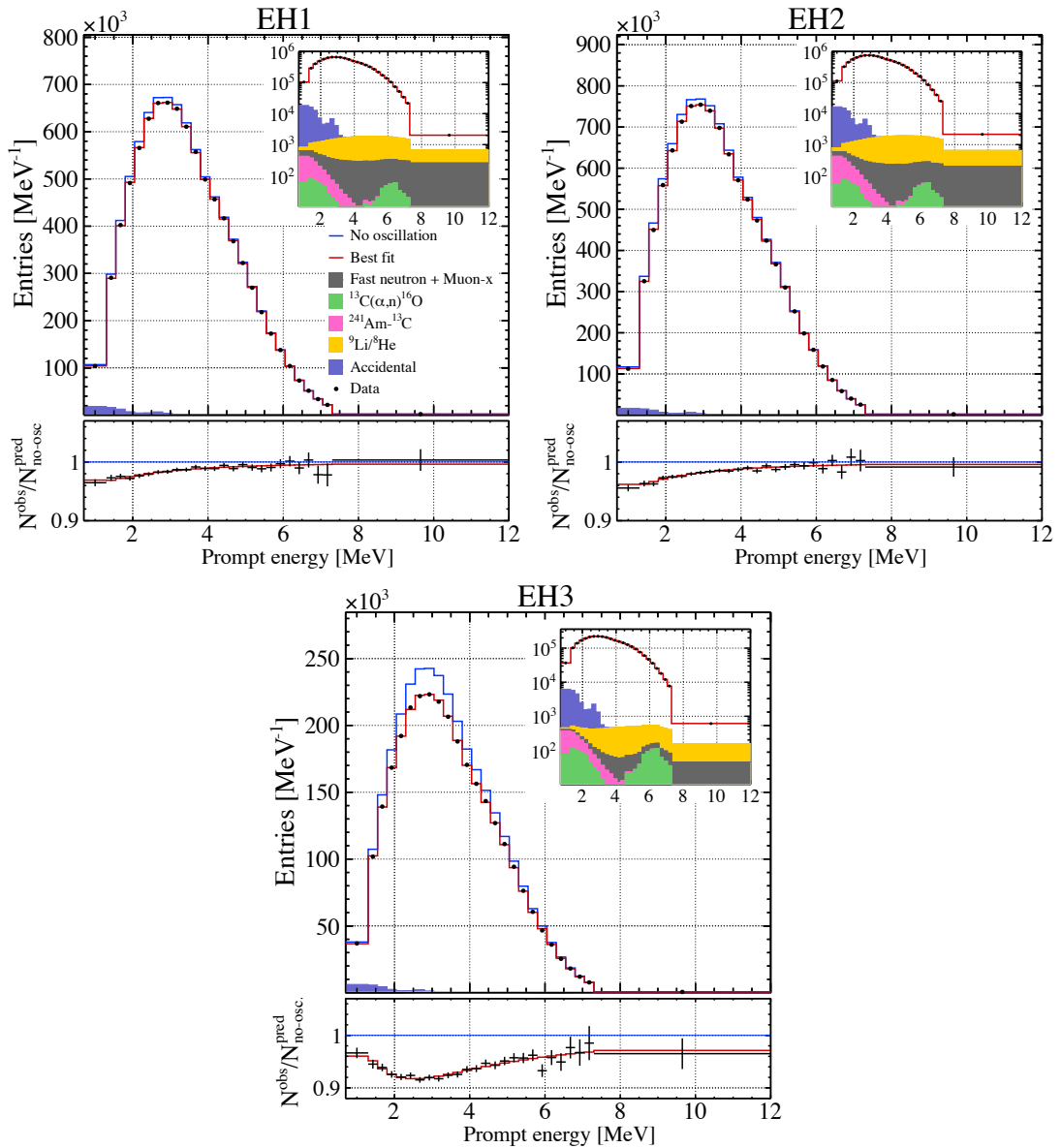


Figure 3.6: The measured positron energy spectra with the best-fit and no-oscillation curves superimposed in the upper panels. The shape of the backgrounds are apparent in the spectra with a logarithmic ordinate shown in the insets and the lower panels shows the ratio of the observed spectrum to the predicted no-oscillations distribution [22].

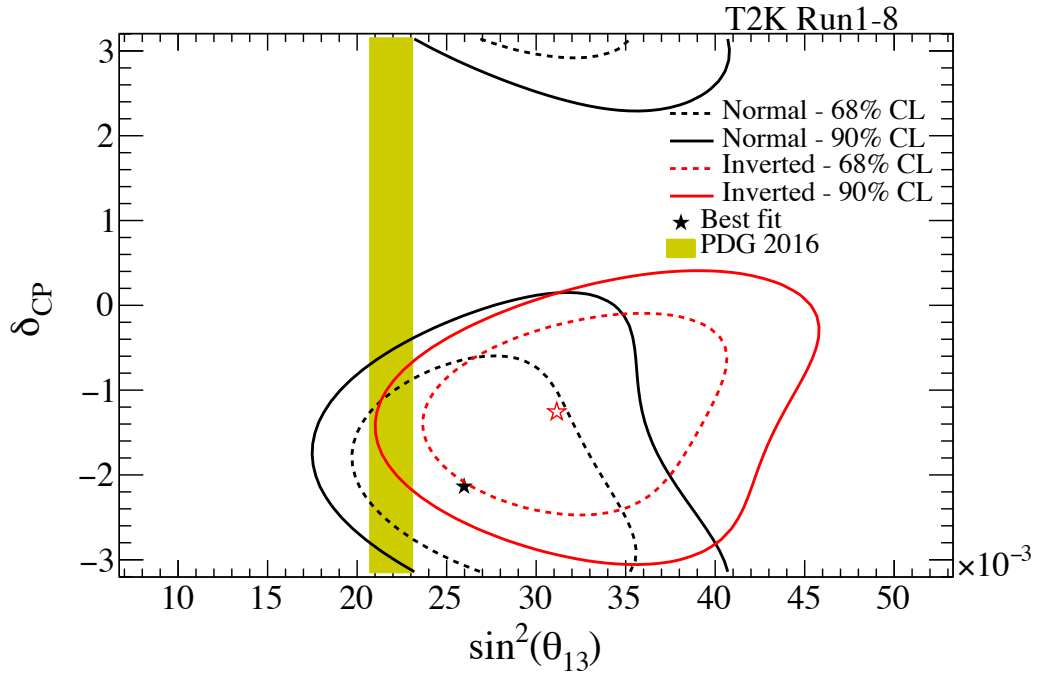


Figure 3.7: Marginalised $\sin^2 \theta_{13} - \delta_{CP}$ posterior distribution for normal mass hierarchy (black) and inverted mass hierarchy (red) in 68 % and 90 % credible intervals compared to the best PDG $\sin^2 \theta_{13}$ [5].

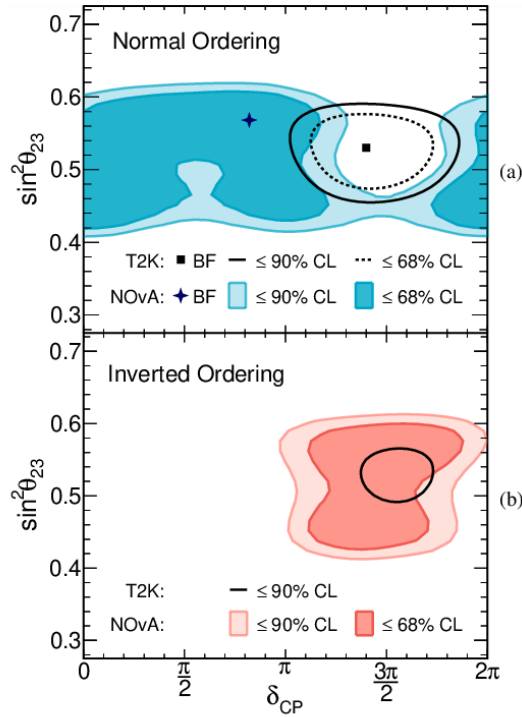


Figure 3.8: 1σ and 2σ confidence level contour $\sin^2 \theta_{13} - \delta_{CP}$ in the a) normal mass ordering and b) inverted mass ordering. Coloured contours correspond to $NO\nu A$ result and black solid and dashed line correspond to the T2K results. [27]

Chapter 4

Prediction of Neutrino Flux at Hyper-Kamiokande

Main task of the thesis was to numerically predict the neutrino fluxes from the atmosphere with basic model of creation, calculate the oscillated fluxes through the approximated Earth with more accurate model of creation atmospheric neutrinos, predict the number of measured events measured for future the Hyper-Kamiokande experiment and compare it with its precursor Super-Kamiokande.

The reason, why atmospheric neutrinos will continue playing key role in the neutrino physics, is the following. The sensitivity of the Hyper-K is shown in the Fig. 4.1. We can see, that the accelerator neutrinos measurement of the Hyper-K are degenerated in the δ_{CP} phase and mass ordering uncertainty. Atmospheric neutrinos measurements can cancel this degeneracy and help to increase the sensitivity for δ_{CP} and mass ordering measurement of the Hyper-K.

Atmospheric neutrinos are also important for studying the neutrino oscillation and its parameters, especially the $\sin^2 \theta_{23}$ and Δm_{23}^2 region. The energy spectrum is relatively wide, from approximately 0.1 GeV to 10^4 GeV. The detected neutrino events can be sorted to the energetic regions and compared with each other and the oscillation parameters can be extracted. The other aspect of atmospheric neutrinos is definitely the range of distances, which can be obtained for different directions of incoming neutrinos (approximately from 30 km to 12000 km). But, at first let us describe process of creation of atmospheric neutrinos and their properties.

The radiation from outer space has variety of energies and it is composed of multiple particle types. The highest energetic radiation (called ultra-high-energy cosmic ray abbreviated UHECR) has energies around PeV = 10^{18} eV and higher. The UHECR is mainly composed from protons, or heavier nuclei (such as α -particles, etc). This particles create a large particle shower, when they collide with molecules of the atmosphere. In this particle shower, mesons (mainly pions and kaons) are produced and they decay relatively quickly with an emission of the e or μ and corresponding antineutrino (or neutrino, what depends on the charge of decayed meson), for example $\pi^+ \rightarrow \mu^+ + \nu_\mu$. Every created muon decays to the muon neutrino, electron and electron antineutrino. When we sum up the number of created neutrinos, we can find out, that approximately two thirds are ν_μ and one third is ν_e (and similarly for antineutrinos).

When UHECR enters the Earths magnetosphere, magnetic field is changing

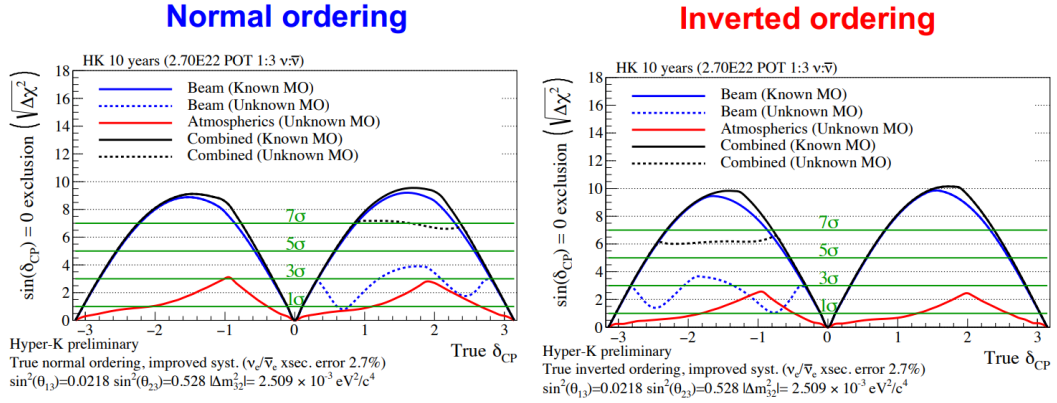


Figure 4.1: A sensitivity dependence of the Hyper-Kamiokande experiment on the δ_{CP} measurement [29]. The graph shows, that separated accelerator and atmospheric neutrinos measurements are not as sensitive as measurements combined. Atmospheric neutrinos measurement takes down the degeneracy of δ_{CP} and mass ordering for accelerator neutrinos measurement.

particles trajectory, so there is created more atmospheric neutrinos around a magnetic poles of the Earth, thus the direction of incoming neutrinos becomes important. After taking into account other more effects (examples), a more accurate model of creation arises. One of this type of accurate models is made by Honda et al. [30], for example. This model was used for the predictions in following sections.

Another problem with computation neutrino oscillation of atmospheric neutrinos is the matter effect. The neutrinos coming from above the horizon, can travel through the ground with different densities and for different distances. The simulation should figure out, if this effect is important enough for taking into account for future analysis. Lets take a look at the steps of the simulation.

4.1 Production of Neutrinos in the Atmosphere

The important role in atmospheric neutrino physics has the simulation of neutrino fluxes created in the atmosphere. The best way how to briefly understand the basics of the model of atmospheric neutrino fluxes is to start your own prediction. We have made a simplified Monte Carlo model, which is homogeneous and isotropic (meaning every point of the atmosphere creates neutrino flux independent on the direction) at any point of the atmosphere. Created neutrino flux is monoenergetic and composed by the only one neutrino flavour. Points were randomly and uniformly spread out in the atmosphere as it is usual in the Monte Carlo method.

At first, we needed to make the atmosphere as a thick sphere with a height of 30 km above the ground as an approximate average height of the neutrino production covered by points, which are described by spherical coordinates. The uniformity of the points was verified by the visual inspection of the point distribution, which can be seen in the Fig. 4.2 and we can see, that they are uniformly spread without clusters.

Furthermore, we need to compute a continuous flux of neutrinos (shortly just

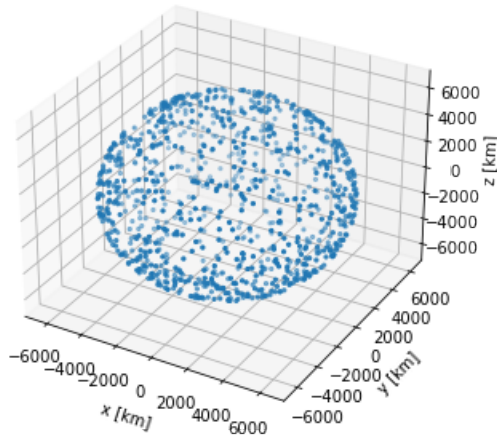


Figure 4.2: Uniform distribution of thousand points of the simulated atmosphere.

the flux) from each point. We can suppose, that flux created by any point is constant and it is decreasing with the square of the distance. An important information of the measurement is direction from which the neutrino came and this is expressed by two coordinates: φ azimuth angle and θ zenith angle. For this purposes is the flux divided into so called bins, each corresponding to particular range of $\cos\theta$ value and for $\varphi \in \langle 0, 2\pi \rangle$. When we make all mentioned steps and the result can be seen in the Fig. 4.3.

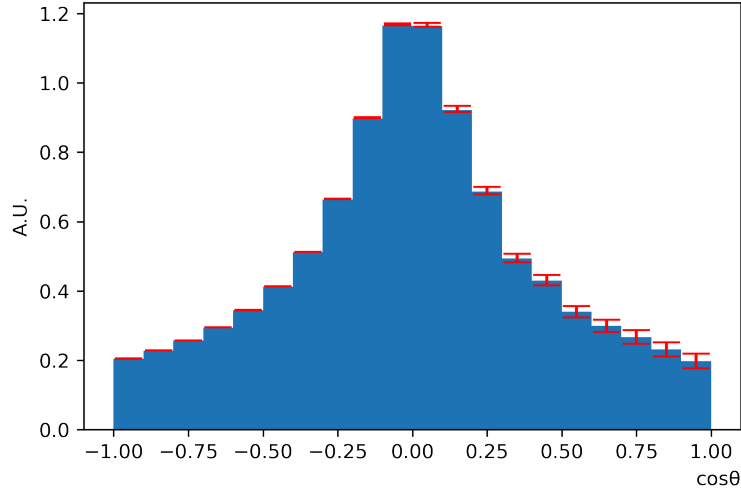


Figure 4.3: Monte Carlo simulation of the non-oscillated flux with isotropic and homogeneous model of neutrino creation for 10^8 points and equidistant intervals in the $\cos\theta$. As it can be seen, the uncertainty of the prediction is much lower for the above horizon part of atmosphere (because of small number of points in those bins).

We can see, that the flux is almost symmetrical, but the above the horizon part ($\cos\theta \in \langle 0, 1 \rangle$) are burdened with a larger statistical error, thanks to less points laying in individual bins due to the geometry of the situation, so the possible differences could be caused by this statistical deviation. It is interesting,

that the maximum of the incoming neutrinos is around the horizon (comparing for example μ 's coming from above in most of cases).

As it has been said earlier, this homogeneous isotropic model is very primitive and does not include the effect of the earth magnetic field changing the trajectory of particles to the magnetic poles. Therefore, we use in the following computations the Honda et al. [30] model which does not suppose the homogeneous and isotropic neutrino creation in the atmosphere. The model provides differential fluxes $\frac{d\Phi}{dE}$ specified in the $\left[\frac{d\Phi}{dE}\right] = (\text{m}^2 \cdot \text{sec} \cdot \text{sr} \cdot \text{GeV})^{-1}$ units and they are provided for each flavour (for ν_e , ν_μ , $\bar{\nu}_e$ and $\bar{\nu}_\mu$), depends on the zenith angle θ (i.e. angle between the neutrino trajectory and vertical direction) similar to our simulation [31]. The values are provided for twenty bins equidistantly divided in $\cos\theta$. Provided differential fluxes depend on the φ azimuth angle as well, but this dependence was not important for our purposes, so we summed up all differential fluxes over the φ .

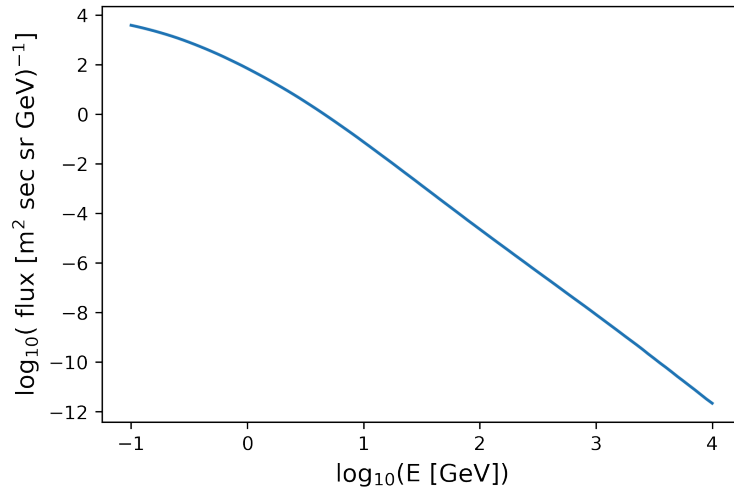


Figure 4.4: An example of the differential flux dependence on the energy for a particular bin for electron neutrinos of the prediction model. For other flavours and other bins the picture is qualitatively the same.

The model energetic spectrum data ranges from 0.1 GeV up to 10^4 GeV equidistant in the logarithmic scale with hundred values and the differential flux is rapidly decreasing with the energy, as can be seen in the Fig. 4.4. However, the differential fluxes for more than about 100 GeV are almost negligible. Despite that all values were considered in calculations.

4.2 Probability, Oscillation Parameters and Matter Effect

The next step was implementing the probabilities from the Eq. (2.17). It was necessary to implement the probability computation as Eq. (2.11) from an amplitude defined in Eq. (2.8) instead of exact probability definition at Eq. (2.17). The reason of this approach will be mentioned later at the computation of the probabilities for neutrinos flying through various densities in the Earth. The

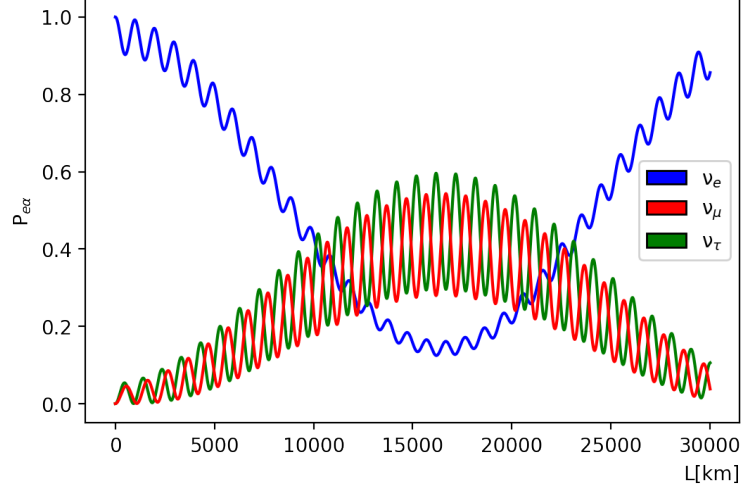


Figure 4.5: Implemented probability of $P(\nu_e \rightarrow \nu_\alpha)$ with $E = 1.4$ GeV, example of the probability dependence on the distance L in vacuum. Oscillation parameters used for computation can be seen at Tab. 2.1.

result can be visually checked as shown in the Fig. 4.5 for vacuum oscillations. The input information for this particular calculation was the energy $E = 1$ GeV, vacuum oscillation parameters, which can be seen in the Tab. 2.1, $\delta_{CP} = 0$ and normal mass ordering. In all text we will consider $\delta_{CP} = 0$ and normal mass ordering unless otherwise stated. This choice of parameters does not have an impact on the following results, since atmospheric neutrinos are very little sensitive to those.

The more challenging part was the computation of oscillation parameters in matter. As it has been discussed earlier, neutrinos oscillate in matter differently, because of the the electrons present. The interaction of neutrino with electron brings a potential similarly as it can be seen in Eq. (2.25) with an adjustment for three neutrino framework as

$$\begin{aligned}
 i \frac{d}{dt} \begin{pmatrix} |\nu_e\rangle \\ |\nu_\mu\rangle \\ |\nu_\tau\rangle \end{pmatrix} &= (U^\dagger \hat{H} U + V) \begin{pmatrix} |\nu_e\rangle \\ |\nu_\mu\rangle \\ |\nu_\mu\rangle \end{pmatrix} = \left[U^\dagger \left(E + \frac{m_1^2}{2E} \right) \mathbb{I} U + \right. \\
 &+ \frac{1}{2E} U^\dagger \begin{pmatrix} 0 & 0 & 0 \\ 0 & \Delta m_{21}^2 & 0 \\ 0 & 0 & \Delta m_{31}^2 \end{pmatrix} U + \begin{pmatrix} V_e & 0 & 0 \\ 0 & V_\mu & 0 \\ 0 & 0 & V_\tau \end{pmatrix} \left. \right] \begin{pmatrix} |\nu_e\rangle \\ |\nu_\mu\rangle \\ |\nu_\tau\rangle \end{pmatrix} = \\
 &= \left[U^\dagger H_0 \mathbb{I} U + \frac{1}{2E} U^\dagger \begin{pmatrix} 0 & 0 & 0 \\ 0 & \Delta m_{21}^2 & 0 \\ 0 & 0 & \Delta m_{31}^2 \end{pmatrix} U + \begin{pmatrix} \Delta V & 0 & 0 \\ 0 & 0 & 0 \\ 0 & 0 & 0 \end{pmatrix} \right] \begin{pmatrix} |\nu_e\rangle \\ |\nu_\mu\rangle \\ |\nu_\tau\rangle \end{pmatrix},
 \end{aligned} \tag{4.1}$$

where $H_0 := E + \frac{m_1^2}{2E} + V_\mu$.

The potentials V_μ and V_τ are equal, that was used in the second line of the Eq. (4.1), because the ν_μ and ν_τ interact with an electron only by so called neutral current what means, that the only Z^0 boson is a mediator particle of this interaction. On the other hand, electron neutrino can interact via charged current and its potential is different from former potential (thus $\Delta V \equiv V_e - V_\mu = 2\sqrt{2}G_F E N_e$, same as in the Sec. 2.5). The first term is proportional to the identity

matrix and again, takes no role in the oscillations. When we plug in the PMNS matrix (defined in Eq. (2.22)) we obtain the matrix quite complicated matrix and it does not seem to be good idea to diagonalize it analytically, but it is possible numerically as

$$\begin{pmatrix}
c_{12}^2 s_{13}^2 (s_{23}^2 \Delta m_{21}^2 + c_{23}^2 \Delta m_{31}^2) - c_{12} s_{12} s_{13} s_{23} c_{23} \Delta m_{32}^2 e^{i\delta} - & s_{12} s_{13}^2 (s_{23}^2 \Delta m_{21}^2 + c_{23}^2 \Delta m_{31}^2) - s_{12}^2 s_{13} s_{23} c_{23} \Delta m_{32}^2 e^{i\delta} \\
-s_{12} c_{12} s_{13} s_{23} c_{23} \Delta m_{32}^2 e^{-i\delta} + s_{12}^2 (c_{23}^2 \Delta m_{21}^2 + s_{23}^2 \Delta m_{31}^2) + & c_{12}^2 s_{13} s_{23} c_{23} \Delta m_{32}^2 e^{-i\delta} - c_{12} s_{12} (c_{23}^2 \Delta m_{21}^2 + s_{23}^2 \Delta m_{31}^2) \\
2E\Delta V & \\
c_{12} s_{12} s_{13}^2 (s_{23}^2 \Delta m_{21}^2 + c_{23}^2 \Delta m_{31}^2) + c_{12}^2 s_{13} s_{23} c_{23} \Delta m_{32}^2 e^{i\delta} - & s_{12}^2 s_{13}^2 (s_{23}^2 \Delta m_{21}^2 + c_{23}^2 \Delta m_{31}^2) + s_{12} c_{12} s_{13} s_{23} c_{23} \Delta m_{32}^2 e^{i\delta} \\
-s_{12}^2 s_{13} s_{23} c_{23} \Delta m_{32}^2 e^{-i\delta} - s_{12} c_{12} (c_{23}^2 \Delta m_{21}^2 + s_{23}^2 \Delta m_{31}^2) & + c_{12} s_{12} s_{13} s_{23} c_{23} \Delta m_{32}^2 e^{-i\delta} + c_{12}^2 (c_{23}^2 \Delta m_{21}^2 + s_{23}^2 \Delta m_{31}^2) \\
-c_{12} s_{13} c_{13} (s_{23}^2 \Delta m_{21}^2 + c_{23}^2 \Delta m_{31}^2) e^{i\delta} + s_{12} c_{13} s_{23} c_{23} \Delta m_{32}^2 & s_{12} s_{13} c_{13} (s_{23}^2 \Delta m_{21}^2 + c_{23}^2 \Delta m_{31}^2) e^{i\delta} - c_{12} c_{13} s_{23} c_{23} \Delta m_{32}^2 \\
-c_{12} s_{13} c_{13} (s_{23}^2 \Delta m_{21}^2 + c_{23}^2 \Delta m_{31}^2) e^{-i\delta} + s_{12} c_{13} s_{23} c_{23} \Delta m_{32}^2 & \\
s_{12} s_{13} c_{23} (s_{23}^2 \Delta m_{21}^2 + c_{23}^2 \Delta m_{31}^2) e^{-i\delta} - c_{12} c_{13} s_{23} c_{23} \Delta m_{32}^2 & \\
c_{13}^2 (s_{23}^2 \Delta m_{21}^2 + c_{23}^2 \Delta m_{31}^2) &
\end{pmatrix} \rightarrow U_m^\dagger \begin{pmatrix} m_{1m}^2 & 0 & 0 \\ 0 & m_{2m}^2 & 0 \\ 0 & 0 & m_{3m}^2 \end{pmatrix} U_m. \tag{4.2}$$

We gain the effective oscillation parameters in matter, effective mass as eigenvalues of the matrix and the mixing angles from the parameterization of the U_m matrix. The effective parameters depend (due to the potential) on the energy of neutrinos and on the relative number of electrons in matter, which can be estimated from a density of the matter in each layer of the Earth model.

The effective parameters can be plugged in the above mentioned Eq. (2.17) and it can be used for computation of oscillation probability of any flavour. Let us have a closer look at the effective mass parameters computation. The numerical results can be seen in the Fig. 4.6 and they corresponds with results from the .

In the obtained oscillation parameters it can be seen the resonance in Mikheyev Smirnov Wolfenstein effect already mentioned in the previous text. The both effective squared mass difference and all three mixing angles changes their value significantly for two particular densities for given energy and for normal ordering. At these special conditions is the neutrino mixing maximal and the effective mass state will flip to the one mass state and stays there. This so called resonance densities can be also identified in the Fig. 4.6 as two points, where $\sin^2 2\theta_{12}$ and $\sin^2 2\theta_{13}$ reach to 1.

4.3 The Earth Model and the Oscillated Fluxes

The atmospheric neutrinos travel through the Earth from some directions and we should take it into account. The real Earth is complex, generally not spherically symmetrical and densities are continuous. For our calculation the Earth was approximated as a spherically symmetrical ball divided to five layers with constant density. The atmosphere was approximated to infinitely thin sphere thirty kilometers above the surface.

The density of electrons in matter was estimated from the density of the matter as number of nucleons in the unit volume divided by two, supposing negligible mass of an electron and identical amount of protons and neutrons. Densities and layer radii were approximated based on the PREM (Preliminary reference Earth model) [32]. PREM models the Earth as the sphere-shaped body with the radial

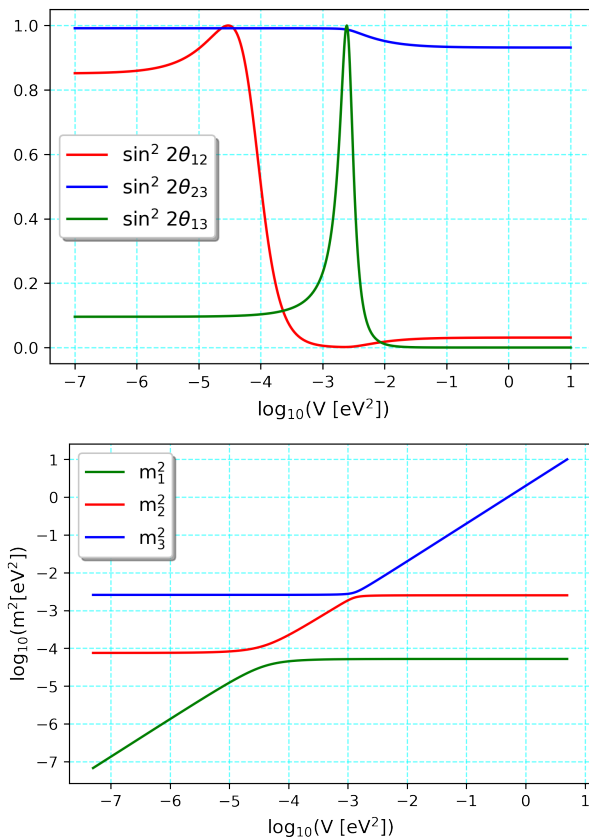


Figure 4.6: The example of gained effective oscillation parameters gained by diagonalization for the normal ordering for an example energy $E = 1$ GeV. Oscillation parameters used for computation can be seen at Tab. 2.1 except the $\delta_{CP} = 0$.

dependence of the elastic properties, pressure, gravity and average density. We will need only the density of the Earth, so it is the only parameter discussed in the text. However, the radial dependence of the density is continuous, it would be difficult to include it into the numerical calculation. Thus we approximated the Earth with the five spherically symmetrical layers with the constant density. The selected numerical parameters (density and radius of the for every layer) are reported in the Tab. 4.1. The comparison of our Earth model with PREM is shown in Fig. 4.7.

Layer	External radius [km]	Used density [$\text{g}\cdot\text{cm}^{-3}$]
inner core	1216	13
outer core	3487	11
inner mantle	5700	5
outer mantle	6358	3.6
lithosphere	6378	2.3
atmosphere	6408	0

Table 4.1: The parameters describing the used spherical symmetrical Earth layer model according to PREM.

As it can be seen in Eq. (2.8) the oscillation amplitude depends not only on energy and oscillation parameters, but on travel distance in each density layer

as well. The distances were determined using basic trigonometry calculus, as it is sketched in Fig. 4.8 so the details of this computation are considered to be technical, thus they will not be discussed in the text. One thing should be mentioned here, that the distances L_j depend on the the zenith angle θ .

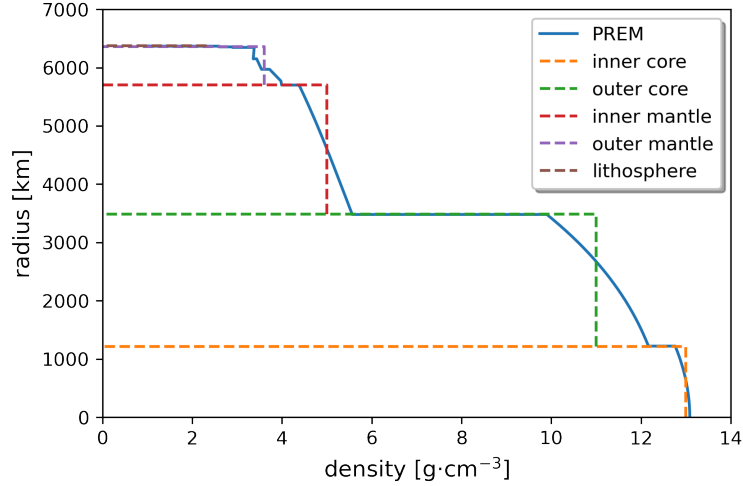


Figure 4.7: Radial density dependence according to the PREM model. Dashed lines indicates the radii and densities for our simplified Earth model.

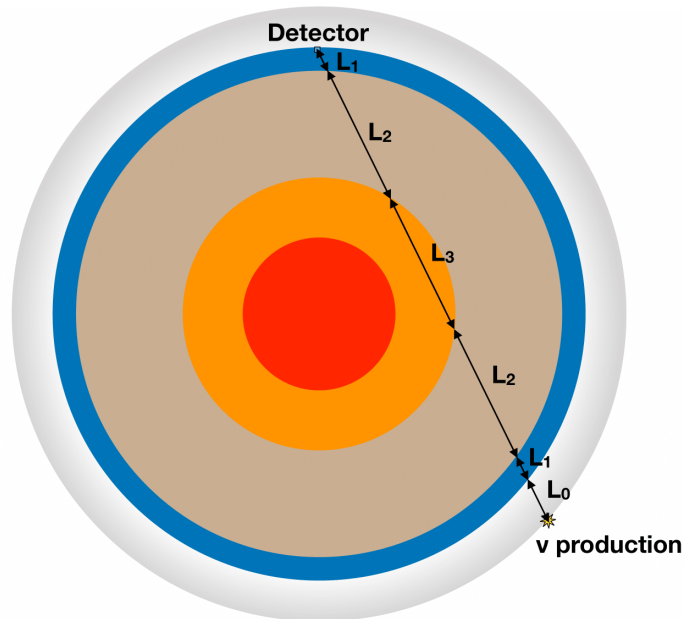


Figure 4.8: The scheme of the neutrino trajectory through the multi-layer Earth. The picture is not up to scale and number of layers is just indicative, too.

Every input information needed for computation for the fluxes was gained, so let us describe the process of the fluxes determination. It was important to compute oscillation parameters in matter for every energy and for every layer density. The oscillated flux of the flavour α was calculated according to the

scheme

$$\frac{d\Phi_\alpha(\theta, E)}{dE} = \sum_{\beta=e,\nu,\tau} \left| A(L_1, \rho_1, E) \dots A(L_i, \rho_i, E) \dots A(L_1, \rho_1, E) A(L_0, \rho_0, E) \right|_{\alpha\beta}^2 \quad (4.3)$$

$$\frac{d\Phi_\beta^{init}(\theta, E)}{dE} = \sum_{\beta=e,\nu,\tau} P_{\alpha\beta} \frac{d\Phi_\beta^{init}(\theta, E)}{dE},$$

where i is number of the deepest layer, which the neutrino travel through, for corresponding θ angle and counted from the surface ($i = 1$ for the lithosphere and so on), L_j is the distance which the neutrino travel in the j -th layer and ρ_j is density of the layer. The L_0 and ρ_0 are parameters for the atmosphere part of path. The $\frac{\Phi^{init}}{dE}$ is the predicted differential flux used as an input and it is arranged to the three-dimensional vector and the $A(L_j, \rho_j, E)$ are 3 by 3 amplitude matrices multiplied to each other for probability matrix computation according to the Eq. (2.9).

In addition, each bin was (equidistantly in the $\cos \theta$) divided into ten smaller bins and one tenth of the whole $\frac{d\Phi_\alpha(\theta, E)}{dE}$ was assigned to each bin, what practically means that ten times more trajectories through the Earth and ten times more oscillations were computed. The data was less randomly determined for directions where trajectories were really close to the borderline of the neighbour layers.

4.4 The Hyper-Kamiokande Experiment

The aim of our computation is to provide rough simulations of the Hyper-Kamiokande results. It is important to understand the detector phenomena, which (some of them) will be included to our computation. But before that, let us describe the experiment itself in more detail.

Hyper-K is, similarly as Super-K, the next-generation water Cherenkov detector under construction with expected start of data taking in 2028 [8]. The basic comparison can be seen in the Tab. 4.2. The water tank will be built in the cavern 650 m under the ground (corresponding to the 1750 m of water equivalent overburden), because of the atmospheric muon shielding, as it is usual in the neutrino measurements. The water tank will be cylindrical shape having 71 m in height and 68 m in diameter with the volume of 258 kt of water. Similarly as the Super-K, the main water tank will be divided to two parts, inner detector (corresponding to 217 kt of water volume) and outer veto region.

In the inner detector there will be installed 20,000 PMTs with 50 cm in diameter and they will provide 20% of the area coverage. In comparison with the Super-K, newer PMTs will have twice the photon efficiency and better timing resolution (2.6 ns FWHM).

The outer veto region will differentiate between particles created in inner detector and coming from outside. The outer detector will be optically separated from the inner part of the detector and outer detector will be made up 10,000 outward looking PMTs with 8 cm in diameter. The outer detector will be lined with highly reflective Tyvek to increase photon collection efficiency.

However, the important value for us is the 217 kt, the detector has some efficiency given by the limits of the particles resolution. To be more specific,

Parameter of the Experiment	Super-K [15]	Hyper-K [8]
Total ultrapure water mass [kt]	50	258
Fiducial mass [kt]	22.5	188
Cylinder size H×D [m×m]	41.4 × 39.3	71 × 68
PMTs coverage (inner detector)	40%	20%
PMTs FWHM time resolution [ns]	6.73	2.6
Overburden in mass water equivalent [m.w.e]	2,700	1,750

Table 4.2: The parameters describing differences between Super-Kamiokande and Hyper-Kamiokande.

when the particle is created too close to the side of the experiment, it may not be included to the measurement. Thus, it is need to establish so called fiducial mass, the effective mass used as target of detectable neutrinos independent on the neutrinos energy. The effectiveness is relatively complicated unknown in general and it depends on the energy due to the bigger volume around the sides where neutrino is not included and on the direction of incoming neutrino taking into apart the shape of the detector (among other more complicated phenomena). For our purposes we will consider efficiency independent on the energy and direction of the neutrinos and we will take it into apart by particular coefficient.

4.5 Fluxes, Predicted Number of Events and Discussion

After finishing all previous steps, the final oscillated differential fluxes were calculated. As it can be seen in Eq. (4.3) the obtained differential fluxes are still dependent on the energy and they should be integrated as

$$\Phi_{\alpha}(\theta) = \int_{E_{\min}}^{E_{\max}} \frac{d\Phi_{\alpha}(\theta, \tilde{E})}{d\tilde{E}} d\tilde{E}, \quad (4.4)$$

where \tilde{E} is a label for integration energy. Unfortunately, the oscillated differential fluxes gained in previous part are discrete values and it is need to be interpolated before the integration. The interpolated function $f(E, \alpha, \cos \theta)$ is gained for every bin and for every (anti)neutrino flavour and it represents the dependence of the flux on the energy. The total fluxes were gained by numerical integration symbolically expressed as

$$\Phi_{\alpha}(\theta) = \int_{E_{\min}}^{E_{\max}} f(E, \alpha, \cos \theta) dE. \quad (4.5)$$

By the inspiration from the Super-K results (at the Fig. 3.2), fluxes were divided into three energetic regions, because we will not need continuous dependence on the energies. The energetic regions were defined by integration boundaries E_{\min} and E_{\max} . The boundaries are $E_{\text{low}} \in \langle 0.1 \text{ GeV}, 0.4 \text{ GeV} \rangle$ for low energy neutrinos, $E_{\text{upper}} \in \langle 0.4 \text{ GeV}, 1.4 \text{ GeV} \rangle$ for upper energy neutrinos and $E_{\text{multi}} \in \langle 1.4 \text{ GeV}, 10^4 \text{ GeV} \rangle$ for multi GeV neutrinos. Now it is time to include the Cherenkov detector resolution.

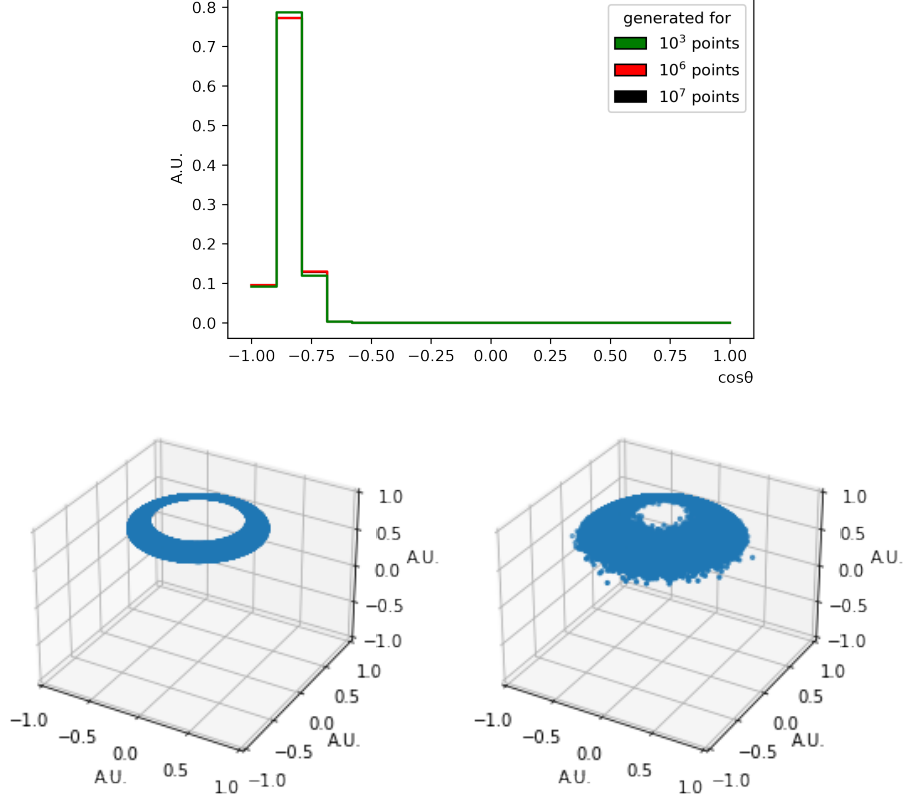


Figure 4.9: An example of the smearing function at the top figure computed for $\sigma_\theta = 5^\circ$. Bottom figures show visualisation of the generated (bottom left) and shifted (bottom right) points in the second bin i.e. $\cos\theta \in (0.9, 0.8)$ for 10^5 points.

The water Cherenkov detector has a finite precision in the incoming neutrino direction reconstruction, so called angular resolution. That practically means, that some neutrinos are assigned to a different bin, than which it really belongs. Therefore, predicted fluxes of incoming neutrinos in each bin will be smeared (i.e. distributed into the neighbor bins) by particular distribution. We cannot assume the normal distribution in θ , but we will compute our own let say smearing functions by the following method.

For each bin we create randomly and uniformly spread points and each point is shifted to the random direction and distance. As it can be seen in the Fig. 4.9 for the example function for various number of points. We can see that for $N = 10^7$ points are statistical fluctuations negligible and the result is almost identical as for $N = 10^6$ points. The direction of the shift is generated by the uniform distribution, but the distance (measured at the surface of the sphere) is generated by the normal distribution, defined by the σ_θ parameter, so called direction reconstruction uncertainty. We considered a value of $\sigma_\theta = 10^\circ$ and $\sigma_\theta = 5^\circ$ similar to Super-K resolution.

The sphere characterize the space of any possible direction. The parameter, which we are interested in, is the $\cos\theta$. New positions of the shifted points is sorted to the corresponding bins and the points distributions are normalised. An example of obtained angular distribution can be seen in the Fig. 4.9 with the visualisation of the points on the sphere. This so called smearing function was

used for oscillated and integrated fluxes. If resolution would be dependent on the energy and direction (taking into account the shape of the experiment as it has been said in Sec. 4.4), the smearing process should be done before the integration, but this computation would take much longer time to calculate the smearing function for each energy. Determination of this dependence would also require complex detector simulation. An example of original oscillated data and smeared data, for upper energy muon neutrinos, is shown in the Fig. 4.10. As we can see, the peaks just distribute to neighbour bins as we expected, while the angular resolution is getting worse.

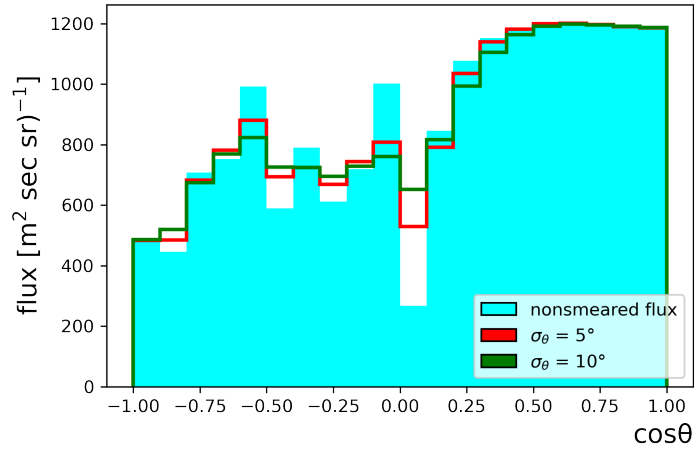


Figure 4.10: The comparison of oscillated nonsmeared and smeared data for $\sigma_\theta = 5^\circ$ and $\sigma_\theta = 10^\circ$. As an example the ν_μ neutrinos are shown for the upper energetic region (0.4 GeV, 1.4 GeV).

This smearing procedure was the last manipulation with the fluxes. Our original intention was the prediction of the number of events detected by the Hyper-Kamiokande experiment. We would in principle convert our gained fluxes to the number of events as

$$N(\cos \theta) = m \times n \times t \int \sigma(E) \frac{d\Phi(E, \cos \theta)}{dE} \epsilon(E, \cos \theta) dE, \quad (4.6)$$

where m is fiducial mass of the detector, n is number of targets in the unit mass, and t is time for how long will the experiment will be taking data, so called exposure time. As it has been said earlier the evaluation of the efficiency and the cross section dependence on energy and zenith angle would require the complex detector simulations of the experiment, so they were approximated by a constant. This simplification is a reason, why our results are only rough estimate. When we qualitatively compare the Super-K data in Fig. 3.2 and our prediction for Hyper-K in Fig. 4.11, we can see, that the Super-K predicted number of events is almost independent on the zenith angle θ (when efficiency is properly taken into account), but our model data still has significant maximum for the neutrinos coming from a horizon.

In order to overcome the troubles with the efficiency and cross section being treated as independent on energy and zenith angle, the number of events for Hyper-K was gained by the linear scaling of the our predicted fluxes to the data

measured by the Super-Kamiokande experiment (for its fiducial mass, number of targets and the exposure time) supposing same cross section and the same efficiency dependence for both experiments (in corresponding energetic regions). The predicted number of events for Hyper-K are thus calculated as

$$N(\cos \theta) = q \int \frac{d\Phi(E, \cos \theta)}{dE} dE, \quad (4.7)$$

where coefficient was estimated as $q = 0.307$ for ν_e and $q = 0.170$ for ν_μ and ν_τ for 10 y of exposure time of Hyper-K (assuming the fiducial volume mass of 190 kt).

Let us discuss the mentioned results from the simulation. The qualitative image should be similar to the Super-Kamiokande results in the Fig. 3.2. We can see, that in our computation of the electron neutrinos, the expected number of events of oscillated neutrinos did not change much from the non-oscillated predictions, similarly as we can see for measured data of Super-K. That does not mean, that electron neutrinos did not oscillated at all. We can extract more information from the simulated data and check the origin of neutrinos measured. We can plot the partial number of events, more accurately speaking, we distinguished neutrino events by their origin. This sort of data are shown in the Fig. 4.12 and we can see, that propagated low energy ν_e are composed from the neutrinos, which oscillated from ν_μ . Also, the ν_μ neutrinos significantly oscillated ν_τ neutrinos. That is the reason why the Super-Kamiokande experiment measured that crucial decrease of the muon neutrinos [15].

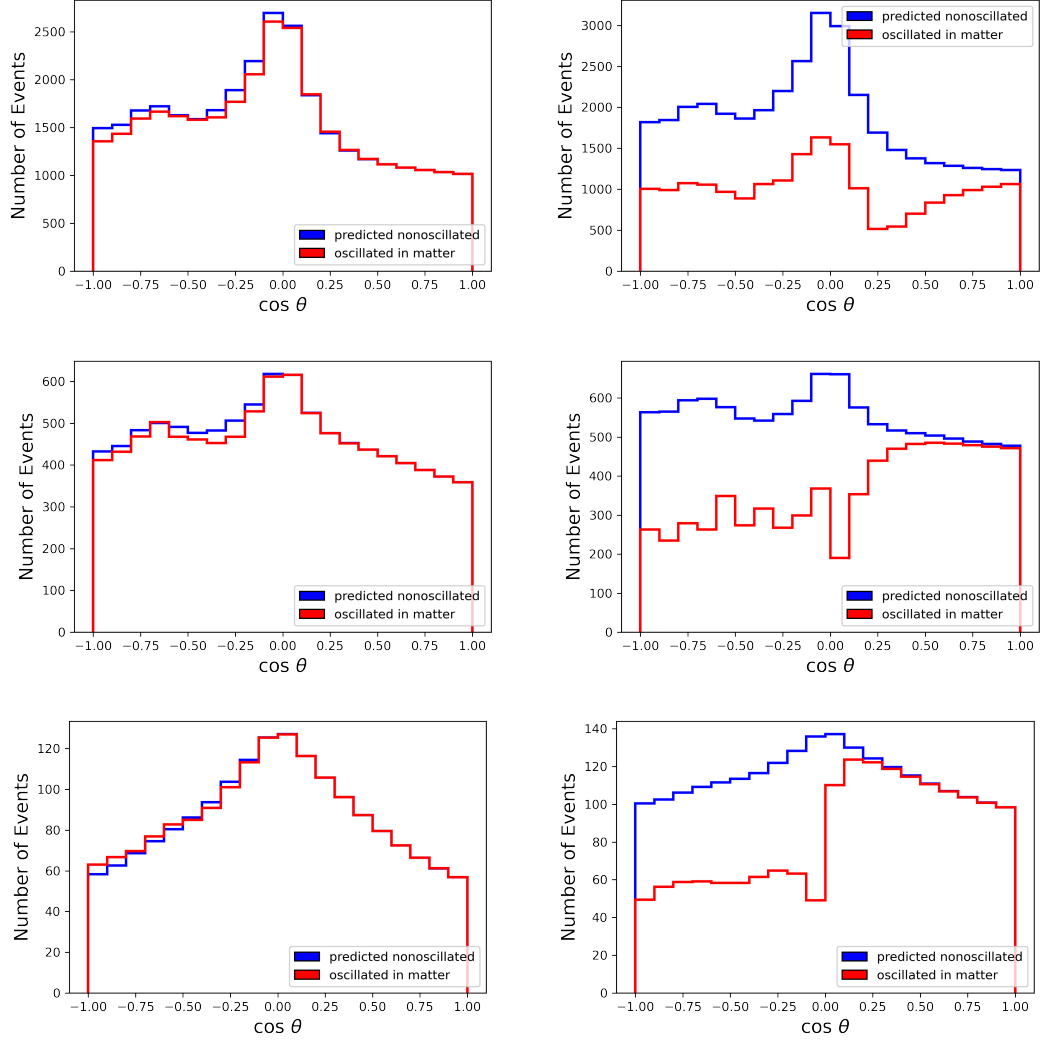


Figure 4.11: The comparison of the predicted number of neutrinos and antineutrinos measured without oscillations and the oscillated number of neutrinos measured. The left part corresponds to the e-like neutrinos and right part to μ -like. Top pictures were calculated for low energetic neutrinos $E_{\text{low}} \in \langle 0.1.4 \text{ GeV}, 0.4 \text{ GeV} \rangle$, middle pictures for upper energetic neutrinos $E_{\text{upper}} \in \langle 0.4 \text{ GeV}, 1 \text{ GeV} \rangle$ and bottom pictures for multi GeV neutrinos with $E_{\text{multi}} \in \langle 1.4 \text{ GeV}, 10^4 \text{ GeV} \rangle$.

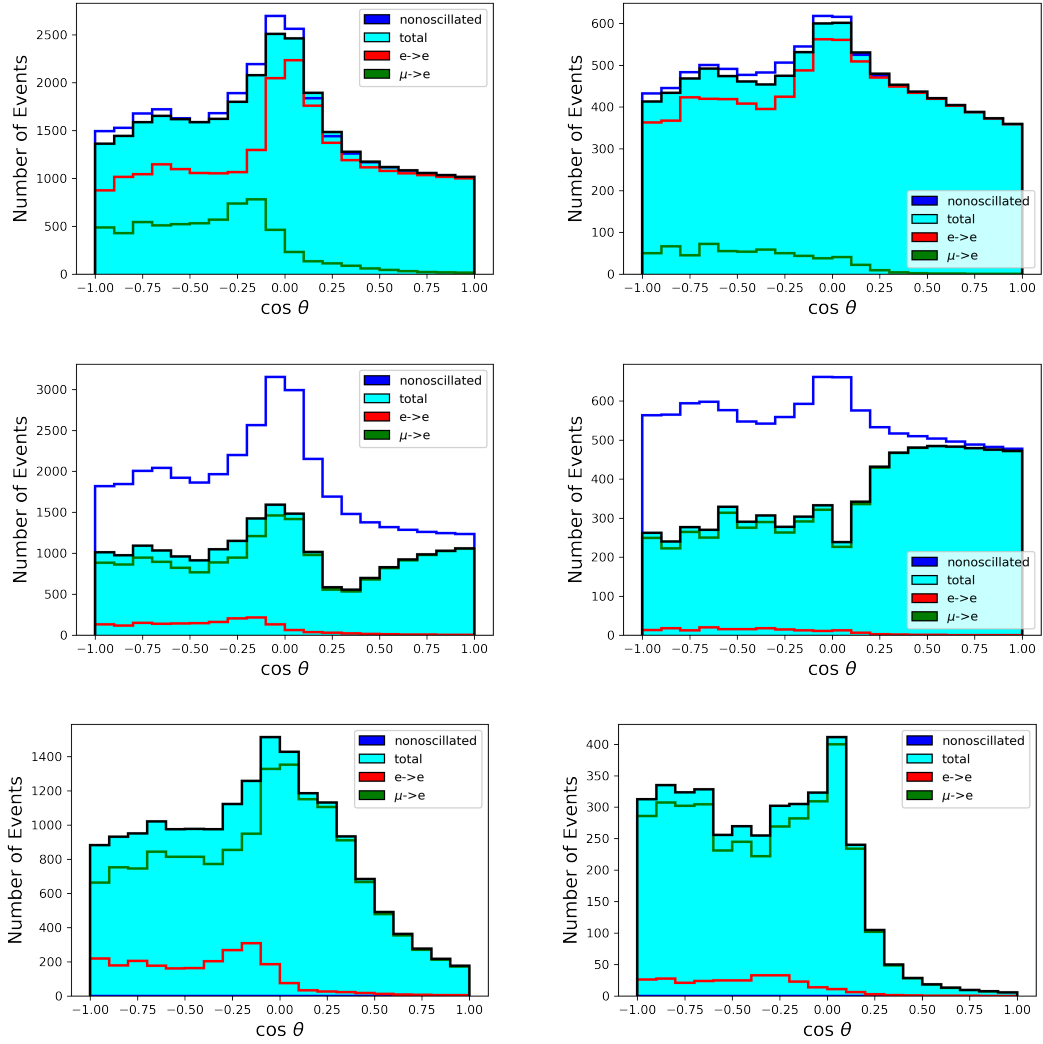


Figure 4.12: The oscillated data distinguished by their origin. The left part corresponds to the lower energetic region (0.1-1.4 GeV) and right part to middle energetic region (0.4-1.4 GeV). Top pictures corresponds to ν_e neutrinos, middle pictures for ν_μ neutrinos and bottom pictures for ν_τ

Chapter 5

Conclusions

Neutrinos play a major role in particle physics today. Their properties are studied through the phenomenon of neutrino oscillation, among others. The focus of this thesis was to study the aspect of the atmospheric neutrino oscillation in the next-generation water Cherenkov experiment Hyper-Kamiokande.

We introduced the basic neutrino mixing and neutrino oscillation formalism in two and three neutrino framework. The neutrino interaction with the mass and MSW effect and computation of the effective oscillation parameters was outlined.

The brief history and prospect of the vacuum oscillation parameters measurement was described with the brief description of the experiments functional principle. The Hyper-Kamiokande experiment and its important role of δ_{CP} in determining was introduced.

After the brief research the simulation method was introduced. We described particular problems with the atmosphere neutrino fluxes prediction, purposed the propagation through the multi layer earth model and the uncertainty of the incoming neutrino reconstruction was included to computation of the fluxes. At the end, the measured number of events was gained for future Hyper-Kamiokande and results were briefly discussed.

Bibliography

- [1] C. L. Cowan, F. Reines, F. B. Harrison, H. W. Kruse, and A. D. McGuire, *Science* **124**, 103 (1956).
- [2] W. C. Haxton, *Annual Review of Astronomy and Astrophysics* **33**, 459 (1995).
- [3] A. Y. Smirnov, The Mikheyev-Smirnov-Wolfenstein (MSW) Effect, in *International Conference on History of the Neutrino: 1930-2018*, 2019, 1901.11473.
- [4] N. Tolich and the SNO collaboration, *Journal of Physics: Conference Series* **375**, 042049 (2012).
- [5] T2K, K. Abe *et al.*, *Phys. Rev. Lett.* **121**, 171802 (2018), 1807.07891.
- [6] M. Aker *et al.*, *Journal of Physics G: Nuclear and Particle Physics* **49**, 100501 (2022).
- [7] Y. Ashie *et al.*, *Physical Review D* **71** (2005).
- [8] Hyper-Kamiokande Working Group, K. Abe *et al.*, A Long Baseline Neutrino Oscillation Experiment Using J-PARC Neutrino Beam and Hyper-Kamiokande, 2014, 1412.4673.
- [9] Particle Data Group, R. L. Workman and Others, *PTEP* **2022**, 083C01 (2022).
- [10] W. Haxton, R. Hamish Robertson, and A. M. Serenelli, *Annual Review of Astronomy and Astrophysics* **51**, 21 (2013).
- [11] J. Boger, R. L. Hahn, and J. B. Cumming, *The Astrophysical Journal* **537**, 1080 (2000).
- [12] A. Y. Smirnov, The msw effect and solar neutrinos, 2003, hep-ph/0305106.
- [13] F. Suekane, T. Iwamoto, H. Ogawa, O. Tajima, and H. Watanabe, An overview of the kamland 1-kiloton liquid scintillator, 2004, physics/0404071.
- [14] S. Abe *et al.*, *Physical Review Letters* **130** (2023).
- [15] Super-Kamiokande, Y. Fukuda *et al.*, *Phys. Rev. Lett.* **81**, 1562 (1998), hep-ex/9807003.

- [16] I. Sokalski, The ANTARES experiment: past, present and future, 2005, hep-ex/0501003.
- [17] F. Halzen and A. Kheirandish, IceCube and High-Energy Cosmic Neutrinos, 2022, 2202.00694.
- [18] T. N. Collaboration and D. Ayres, Nova proposal to build a 30 kiloton off-axis detector to study neutrino oscillations in the fermilab numi beamline, 2005, hep-ex/0503053.
- [19] L. Suter, Neutrino experiment results and prospects for CP violation, Interplay between Particle and Astroparticle physics 2018 (IPA2018), 2018.
- [20] D. Karlen and on behalf of the T2K Collaboration, Universe **5** (2019).
- [21] K. Abe *et al.*, Physical Review D **103** (2021).
- [22] Daya Bay, F. P. An *et al.*, Phys. Rev. Lett. **130**, 161802 (2023), 2211.14988.
- [23] F. An *et al.*, Nuclear Instruments and Methods in Physics Research Section A: Accelerators, Spectrometers, Detectors and Associated Equipment **811**, 133 (2016).
- [24] R. Collaboration and J. K. Ahn, Reno: An experiment for neutrino oscillation parameter θ_{13} using reactor neutrinos at yonggwang, 2010, 1003.1391.
- [25] Nature Physics **16**, 558 (2020).
- [26] F. An *et al.*, Journal of Physics G: Nuclear and Particle Physics **43**, 030401 (2016).
- [27] The NOvA Collaboration, M. A. Acero *et al.*, Phys. Rev. D **106**, 032004 (2022).
- [28] K. W. Group *et al.*, A long baseline neutrino oscillation experiment using j-parc neutrino beam and hyper-kamiokande, 2015, 1412.4673.
- [29] P. Soler, The Hyper-Kamiokande experiment: design, status of construction and physics goals, 31st International Symposium on Lepton Photon Interactions at High Energies, 2023.
- [30] M. Honda, M. Sajjad Athar, T. Kajita, K. Kasahara, and S. Midorikawa, Phys. Rev. D **92**, 023004 (2015), 1502.03916.
- [31] Atmospheric neutrinos model creation, m. honda, <http://web.archive.org/web/20080207010024/http://www.808multimedia.com/winnt/kernel.htm>, Accessed: 2022-09-30.
- [32] A. M. Dziewonski and D. L. Anderson, Physics of the Earth and Planetary Interiors **25**, 297 (1981).

List of Figures

3.1	The Standard Solar Model prediction of solar neutrino flux from various creation processes [10]. Thresholds of some solar neutrino experiments are indicated at the top of the graph.	13
3.2	Measured cosine zenith angle distributions of fluxes measured by Super-K for e-like (left) and μ -like (right) neutrinos in three energetic regions, i.e. lower than 0.4 GeV, from 0.4 GeV to 1.4 GeV and above 1.4 GeV (multi-GeV) [15].	15
3.3	Measuring principle used for separating ν_e and ν_μ [19].	16
3.4	Off-axis energy distributions of ν fluxes and corresponding oscillation probabilities of the T2K experiment [20].	16
3.5	Compilation of results of $\sin^2 \theta_{23}$ and $ \Delta m_{32}^2 $ parameters fits for different experiments from 2017 [21].	17
3.6	The measured positron energy spectra with the best-fit and no-oscillation curves superimposed in the upper panels. The shape of the backgrounds are apparent in the spectra with a logarithmic ordinate shown in the insets and the lower panels shows the ratio of the observed spectrum to the predicted no-oscillations distribution [22].	21
3.7	Marginalised $\sin^2 \theta_{13} - \delta_{CP}$ posterior distribution for normal mass hierarchy (black) and inverted mass hierarchy (red) in 68 % and 90 % credible intervals compared to the best PDG $\sin^2 \theta_{13}$ [5]. . .	22
3.8	1σ and 2σ confidence level contour $\sin^2 \theta_{13} - \delta_{CP}$ in the a) normal mass ordering and b) inverted mass ordering. Coloured contours correspond to NO ν A result and black solid and dashed line correspond to the T2K results. [27]	22
4.1	A sensitivity dependence of the Hyper-Kamiokande experiment on the δ_{CP} measurement [29]. The graph shows, that separated accelerator and atmospheric neutrinos measurements are not as sensitive as measurements combined. Atmospheric neutrinos measurement takes down the degeneracy of δ_{CP} and mass ordering for accelerator neutrinos measurement.	24
4.2	Uniform distribution of thousand points of the simulated atmosphere.	25
4.3	Monte Carlo simulation of the non-oscillated flux with isotropic and homogeneous model of neutrino creation for 10^8 points and equidistant intervals in the $\cos \theta$. As it can be seen, the uncertainty of the prediction is much lower for the above horizon part of atmosphere (because of small number of points in those bins).	25

4.4	An example of the differential flux dependence on the energy for a particular bin for electron neutrinos of the prediction model. For other flavours and other bins the picture is qualitatively the same.	26
4.5	Implemented probability of $P(\nu_e \rightarrow \nu_\alpha)$ with $E = 1.4$ GeV, example of the probability dependence on the distance L in vacuum. Oscillation parameters used for computation can be seen at Tab. 2.1.	27
4.6	The example of gained effective oscillation parameters gained by diagonalization for the normal ordering for an example energy $E = 1$ GeV. Oscillation parameters used for computation can be seen at Tab. 2.1 except the $\delta_{CP} = 0$.	29
4.7	Radial density dependence according to the PREM model. Dashed lines indicates the radii and densities for our simplified Earth model.	30
4.8	The scheme of the neutrino trajectory through the multi-layer Earth. The picture is not up to scale and number of layers is just indicative, too.	30
4.9	An example of the smearing function at the top figure computed for $\sigma_\theta = 5^\circ$. Bottom figures show visualisation of the generated (bottom left) and shifted (bottom right) points in the second bin i.e. $\cos\theta \in (0.9, 0.8)$ for 10^5 points.	33
4.10	The comparison of oscillated nonsmeared and smeared data for $\sigma_\theta = 5^\circ$ and $\sigma_\theta = 10^\circ$. As an example the ν_μ neutrinos are shown for the upper energetic region (0.4 GeV, 1.4 GeV).	34
4.11	The comparison of the predicted number of neutrinos and antineutrinos measured without oscillations and the oscillated number of neutrinos measured. The left part corresponds to the e-like neutrinos and right part to μ -like. Top pictures were calculated for low energetic neutrinos $E_{\text{low}} \in \langle 0.1.4 \text{ GeV}, 0.4 \text{ GeV} \rangle$, middle pictures for upper energetic neutrinos $E_{\text{upper}} \in \langle 0.4 \text{ GeV}, 1 \text{ GeV} \rangle$ and bottom pictures for multi GeV neutrinos with $E_{\text{multi}} \in \langle 1.4 \text{ GeV}, 10^4 \text{ GeV} \rangle$.	36
4.12	The oscillated data distinguished by their origin. The left part corresponds to the lower energetic region (0.1-1.4 GeV) and right part to middle energetic region (0.4-1.4 GeV). Top pictures corresponds to ν_e neutrinos, middle pictures for ν_μ neutrinos and bottom pictures for ν_τ .	37

List of Tables

2.1	Measured values of parameters of neutrino oscillations in normal order taken from PDG with $\pm 1\sigma$ [9].	9
4.1	The parameters describing the used spherical symmetrical Earth layer model according to PREM.	29
4.2	The parameters describing differences between Super-Kamiokande and Hyper-Kamiokande.	32